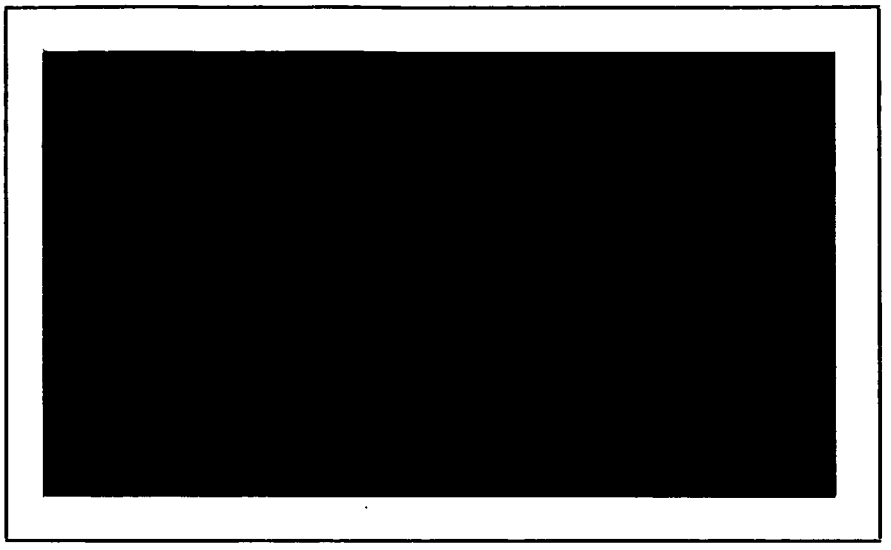

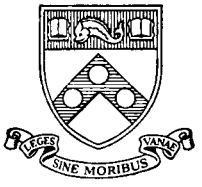

UNIVERSITY OF PENNSYLVANIA

ELECTROCHEMISTRY LABORATORY

PHILADELPHIA, PENNSYLVANIA 19104

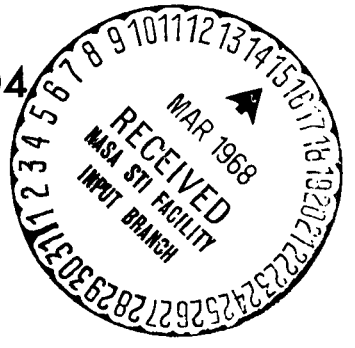

APPENDIX A

of

SEMI-ANNUAL PROGRESS REPORT NO. 11

1 JULY 1967 to 31 DECEMBER 1967

STUDIES IN FUNDAMENTAL CHEMISTRY OF FUEL CELL REACTIONS

NsG-325

Submitted to:

NATIONAL AERONAUTICS AND SPACE ADMINISTRATION

Washington 25, D.C.

Submitted by:

Professor John O' M. Bockris

The Electrochemistry Laboratory
The University of Pennsylvania
Philadelphia, Pa. 19104

NOTICE

This report was prepared as an account of Government sponsored work. Neither the United States, nor the National Aeronautics and Space Administration (NASA), nor any person acting on behalf of NASA:

(a) Makes any warranty or representation, expressed or implied, with respect to the accuracy, completeness, or usefulness of the information contained in this report, or that the use of any information, apparatus, method, or process disclosed in this report may not infringe privately owned rights; or

(b) Assumes any liabilities with respect to the use of or for damages resulting from the use of any information, apparatus, method, or process disclosed in this report.

As used above, "person acting on behalf of NASA" includes any employee or contractor of NASA, or employee of such contractor, to the extent that such employee or contractor of NASA, or employee of such contractor, prepares, disseminates, or provides access to, any information pursuant to his employment or contract with NASA, or his employment with such contractor.

TABLE OF CONTENTS

SECTION V

Work of Mr. J.W. Diggle

(Supervised by Professor A. Despic)

Title of Project: The study of dendritic zinc deposition from alkaline solution.

Long Term Aims: To gain (a) a fuller understanding of the formation of zinc dendrites, (b) a mechanism which adequately describes the experimental behavior, and (c) the ability to apply simple equations to the growth of metal deposits in dendritic, or non-dendritic, form as the system demands.

Specific Aims for This Period: To continue the investigation of the initiation and and propagation of dendritic zinc in systems without previous rigorous purification of solutions used.

This report is based upon a proposed publication which is, at the present time, under preparation.

DENDRITIC DEPOSITION OF ZINC FROM ALKALINE ZINCATE SOLUTIONS

I. INTRODUCTION

The electrocrystallization of deposited zinc in a dendritic form is of importance in the operation of silver-zinc and zinc-air batteries. The dendrites formed upon the zinc electrode during the charging cycle often rupture the electrode separators and cause premature failure by short-circuiting with the other electrode.

The dendritic crystallization of metals has been studied extensively over the last few years, both in the course of electrodeposition and from molten metals. There are several reasons to believe that the dendritic formation in both systems is related to a common reason involving, on the one hand, overpotential as a rate-determining parameter and, on the other, the degree of undercooling. The crystallographic morphology of the dendrites formed in both systems is similar, i.e., growth normal to the substrate surface with secondary and tertiary branching from this main growth axis.

Studies with silver dendrites by Barton and Bockris[1] and Reddy[2] have indicated that a critical overpotential is a necessity for dendrite initiation and that the value is probably related to the establishment of diffusion gradients. Reddy has also suggested that this critical overpotential may be related to the stacking fault energy of the crystal

lattice[3, 4] necessary for the formation of a twin plane, through which the dendrite propagates. The Barton and Bockris theory for dendritic deposition of silver assumed that the transport of material to the dendrite tip was spherical diffusion controlled, so that the rate of growth of a dendrite normal to the silver substrate was determined by the tip radii. However, in order to account for the fact that the rate of growth should then be a maximum at zero tip radius and equal to the rate obtained, for that overpotential, under complete activation control (as is not the case), it was necessary to include the substantial change of the reversible electrode potential at the tip or edge, compared to that of a flat surface, due to the effect of surface energy becoming pronounced at low radius of curvature. In this way a maximum dendrite growth rate would be achieved at some optimum tip radius which is given by

$$r_{opt} = \frac{1 \pm \left[\frac{1 + DC_{\infty}F^2\eta}{2\gamma V i_0}\right]^{\frac{1}{2}}}{\frac{F\eta}{2\gamma V}}$$

where D is the diffusion coefficient of Ag^+, C_{∞} is the bulk concentration of Ag^+, γ is the surface tension between metal and solution, V is the molar volume, and i_0 is the exchange current density.

This equation leads to a value of the maximum growth rate which, when $i_0 \rightarrow \infty$, is proportional to η^2 and when i_0 is low is proportional to η.

Hamilton,[5] assuming that the dendrite tip was a moving paraboloid, has shown that to correlate his equations with the results of Barton and

Bockris, it was necessary to assume (i) a value for the surface tension that was much lower than that used in the Barton and Bockris theory, i.e., 185 erg/cm^2, as against 2,000 ergs/cm^2, (ii) the value of i_0 that was an order of magnitude larger than at macro-electrodes, i.e., 380 A/cm^2 at a concentration of 7.6×10^{-4} moles cm^{-3} as compared to 36 A/cm^2 taken in the Barton and Bockris theory. Hamilton was, however, able to show that the computed values for the tip radius and growth velocity with respect to overpotential were in good agreement with the results from the study of Barton and Bockris. It was concluded that the growth of the dendrites was largely diffusion controlled, and, where the surface tension at the metal-solution interface was low and the i_0 value high, due to a twin plane growth mechanism.

Reddy,[2] in a study of the formation of silver dendrites from molten halides concluded that the dendritic deposition was predominately diffusion controlled. An initiation overpotential of 4 mV was reported (c.f. 3 mV reported by Barton and Bockris), and, in common with Hamilton, a twin plane growth mechanism was supported.

The electrolytic deposition of zinc can occur in several morphological forms dependent upon the conditions of electrodeposition. The three main forms of zinc deposition are (1) compact, (2) spongy or mossy, (3) dendritic, each form being obtained from any other form by a change in electrodeposition conditions. The following table shows under what conditions these three modifications are formed, and how change from one form to another can be facilitated.

TABLE 1

Compact Zinc Deposits C Spongy Zinc S Dendritic Zinc D

Increasing zinc ion concentration	D → S → C
Electrolyte stirring	D → S → C
Increased current density	C → S → D
Increase in electrolyte temperature	D → S → C
Increase in electrolyte viscosity	C → S → D
Increase in zinc overpotential	C → S → D
Pulsating or alternating current	D → S → C
Addition of certain foreign ions	D → S
Presence of free convection	D → S

From Table 1 it can be concluded that dendritic formation is favored by low zinc ion concentration, absence of stirring, increased current density, increased overpotential, low temperature, increased viscosity,[25] and retarded by electrodeposition in the presence of certain foreign ions[6, 7, 8, 9, 10] and by the use of pulsating[13, 14] or alternating current.[11,12] The importance of diffusion gradients in dendritic deposition is thus established; any parameter which favors increased diffusion gradients favors spongy and dendritic deposition and vice versa. The change in the zinc deposition morphology from compact to spongy is of importance in the electrolytic preparation of metal powders, a review of which was published by Ibl[15] in 1962. Apart from this phenomenon being related to diffusional

considerations, other theories have been proposed for morphological changes during metallic deposition, e.g., the concurrent hydrogen evolution theory,[16] oxide formation theory,[17] the presence of colloidal zinc,[18] and the secondary discharge of other cations[19,20] or complex ions.[21] The concurrent hydrogen evolution and secondary discharge of other ions both belong to the same type of secondary deposition —that of homogeneous metal deposition at some point away from the cathode surface in which a non-coherent deposit is obtained. A similar proposal was considered by Călusaru[22] involving the quantum mechanical electron tunnelling effect. At low overpotentials the neutralization distance of an electron is seen as being equal to the zinc lattice parameter, therefore compact zinc deposition occurs at the cathode surface. As the overpotential rises, the neutralization distance was proposed to exceed the lattice parameter so that the electron did not neutralize a zinc ion until some point a short distance from the cathode surface, and so a non-coherent metallic deposit is formed. It was shown for Cu deposition by Atanasiu and Călusaru[23] that although powdery or spongy copper deposition occurs at the limiting current density, it does not do so immediately the limiting current density is reached; a region of approximately 150 mV overpotential at the limiting current density exists before powder formation occurs. This may indicate that the change in morphology from compact to spongy or powder deposition is not totally related to an increased diffusion gradient; analogously, it was uncertain

whether the change from compact to dendritic zinc can be related solely to a deposition mechanism changing from activation to diffusion control, as has been reported.[24]

For the deposition of zinc from alkaline zincate solutions, and also for Cd from $CdSO_4$ solutions, spongy or powdery deposits can be obtained below the limiting current density; so in these cases, the existence of a zero metal ion concentration at the cathode surface is not the determining factor. Ibl[15] has suggested that this powdery deposition occurs by the action of colloidal substances in the electrolyte, e.g., metallic zinc produced by an anodic disintegration reaction similar to those reported by Straumanis et al.[26] This metallic zinc then migrates electrophoretically to areas in which the diffusion gradients are the highest, i.e., those areas which act as peaks upon a microrough surface, and, as deposition proceeds, the surface roughness increases and so powder or spongy metal deposits are formed. Powder deposition will also occur at those areas which do not function as peaks, although the rate of deposition will be lowered; so after the lapse of a certain time complete cathode coverage will be attained due to the two deposition processes outlined above and also by some degree of lateral spreading of the deposit. Thus at complete cathode coverage the deposit thickness would not be expected to be uniform, i.e., calculation of deposit thickness from the coulombs passed and the elapsed time would produce only an average thickness. It is easy to see that some type of relationship should exist between the time

required for complete cathode coverage and the applied current density; Kushner[27] has shown that for Cu deposition from acidified $CuSO_4$ solution (below limiting current density) a hyperbolic relationship exists between current density applied (I) and the time for complete cathode coverage (t). Kushner's results were interpreted, and were in good agreement with, the equation of Evans and Shome[28] relating velocity of lateral spreading of the deposit to the number of nuclei formed, i.e., current density. To conclude, it could be said that the electrodeposition of metals in powdery or spongy modifications is reasonably well understood, although universal agreement has yet to be achieved. However, the case of the dendritic modification, apart from some very basic considerations, very little is known about reasons and mechanisms of their formation. In the Barton and Bockris[1] study of silver dendrites, it was proposed that for spherical diffusion to occur at the dendrite tips, the dendrite precursors must penetrate the original substrate diffusion layer and so form their own local diffusion gradients. However, as Reddy[2] pointed out, this would suggest that as the substrate diffusion layer decreases, the formation of dendrites should increase. It is clear, however, that where the deposition is diffusion controlled, this would not be valid in the case where the substrate diffusion layer was reduced by stirring or natural connection. In the case where the substrate diffusion layer was reduced by reducing the diameter of a spherical substrate,[1] there was a tendency for the number of dendrites to increase as the overall current density increased, i.e., as the substrate diffusion layer decreases. That

dendrites do arise from either protrusions or preferred orientations (facets) has been reported recently by Powers[29] for zinc deposition from alkaline solutions. Krebs and Roe[30] in a study of the electrodeposition of silver from aqueous $AgClO_4$ have shown that the deposition does not occur uniformly, but occurs in the form of hemispherically-shaped deposits which could perhaps be the precursors to dendrites.

Crystallographic studies of dendrite formation have been quite frequent over the last few years, notably that due to Wranglen[31] in which the dendrites were identified as single crystals whose plane of growth corresponded to the closest packed lattice plane. Silver dendrites grown by Yang et al.[32] were examined by Faust and John[33] and identified, not as single crystals, but as a twinned structure. This twinning was proposed to be an integral part of dendritic formation, as mentioned previously with the work of Reddy.[2] The presence of twinned dendritic structures was further supported by work by Ogburn et al.,[34,35,36] Hamilton and Seidensticker,[37] and further work by Faust and John.[38] It should, however, be mentioned that this twinning may be the result of very fast dendritic growth, and therefore not be an essential to the growth mechanism. It is known that the structure of copper, when shock loaded above a minimum value, does show the presence of twins;[39] it may therefore not be unreasonable to expect twinned dendritic structures when high overpotentials (an order or magnitude or more greater than the initiation overpotential), with the resultant fast propagation rate, are applied.

In conclusion, it could be said that there is yet no theory which can adequately explain the reasons for the initiation and all the phenomena associated with dendritic deposition, both in electrodeposition and in the crystallization of molten metals. It is particularly important that any such theory should explain the wide difference between the initiation overpotentials of silver (4 mV) and zinc (≈70 mV), and the ease, in the case of silver, and the difficulty, in the case of zinc, of formation of single dendrites with high propagation rates. In the usual zinc-silver batteries, one normally experiences a large number of dendrites growing in clusters rather than single dendrite formations. (For silver,[1] at overpotentials considerably higher than the initiation value, one or two dendrites only are formed.) It is also of importance to gain a better understanding of the basic causes of dendrite growth, e.g., what significance, if any, can be attached to the so-called initiation times, and what electrodic parameters control the value of the critical overpotential required for dendritic deposition.

II. EXPERIMENTAL

2.1. Electrolyte

The electrolyte used throughout this work was a 10% $\frac{W}{W}$ solution of potassium hydroxide (Baker reagent grade) in conductivity water to which was added sufficient reagent grade ZnO to produce zincate concentrations between 10^{-2} and 0.2 moles liter^{-1}. All electrolytes were

deaerated with purified nitrogen for 4 hours, in the subsidiary cell (see apparatus), prior to flushing through into the observation cell.

No rigorous purification schemes were used for the reagents, since it was desired to approach those conditions of purity prevalent in zinc-silver batteries.

2.2. Electrodes

In order to identify the mode of the diffusion process it was decided that use of spherical zinc electrodes, whose radii could be varied between 0.05 and 0.5 mm, would be advantageous. However, the preparation of these electrodes, from the zinc substrate, yielded some difficult problems due to the very high vapor pressure that zinc possesses at its melting point. Hence, due partly to this problem, and to the low melting point of zinc itself, the following electrode preparation procedure was used: A short length of 0.2 mm diameter platinum wire was sealed into 3 mm bore glass tubing — the length of platinum used being dependent upon the diameter of the electrode sphere required — this platinum wire was then slowly melted and allowed to run back upon itself until a complete sphere had been formed which was in contact with the tip of the glass tubing. Platinum spheres of 1.0 mm diameter prepared in this manner were used throughout this work. Following formation, the platinum sphere was then chemically cleansed in a mixture of sulphuric and nitric acids for five minutes and then washed thoroughly with conductivity water. Microscopic examination of the platinum sphere at this stage showed the surface

to possess high reflectivity and to be void of visible imperfections, etc. The platinum sphere in this condition was then immersed into a strongly agitated solution containing 1 mole/l $ZnSO_4 \cdot 7H_2O$ dissolved in 0.01 N H_2SO_4 and a low overpotential applied (< 50 mV). Under such conditions, where the limiting current density is very high, smooth zinc deposition was always observed. The deposition was continued for ten minutes, after which time, assuming 100% coulombic zinc deposition efficiency, the deposit was calculated as 10^{-3} cm thick. The specimen electrode was then withdrawn from the electrolyte, washed thoroughly in conductivity water, and placed immediately in the experimental cell.

The anode and reference electrodes were prepared in an identical manner, with the exception that the anode electrode spheres were between 2 and 3 mm in diameter and formed to 50μ thickness. The measured difference in the electrode potentials of the cathode electrodes prepared and the reference electrode was always less than 1 mV. Freshly prepared cathode and reference electrodes were used in every experiment, and a freshly prepared anode in every other experiment.

2.3. Apparatus

(i) Cell

The cell, as shown in Figure 1, allows direct observation of the zinc deposition process and also a visual method for the determination

of dendrite growth rates. The electrode assembly E consisted of the three electrodes inserted via glass guide tubes in the cell and then clamped into position with gas-tight Teflon seals. The temperature of the thermostatted outer jacket was maintained at the required temperature (±0.05°C).

(ii) Optical system

The optical tube (A in Figure 1) is basically similar to the arrangement of Barton and Bockris, in which a real image of the spherical electrode is projected onto the objective lens of a microscope system mounted horizontally. This system, which has only one optical window between the lenses and the electrode under observation, avoids the problem of image distortion usually found with externally mounted optical arrangements and thereby increasing both the resolution and the possible magnification range. In this present work, due to problems with illumination, the maximum magnification used was 300×. In future work it is hoped that these problems can be overcome and full use of the optical system be achieved.

Extensive use was made of polaroid photography both to observe morphological changes in the zinc deposit, and to determine the growth of individual dendrites.

(iii) Electronic system

Potentiostatic control was used throughout this work by use of a Wenking potentiostat, to control to overpotential, and a precision

potentiometer with which the applied overpotentials were accurately determined. The system was so arranged that when the potentiometer reading and the overpotential applied by the potentiostat coincided with the overpotential recorded by the electrode under examination (as measured by an electrometer) the whole system was in balance, and this was observed by identical readings upon two ammeters, one in the potentiostat circuit and the other in the potentiometer circuit. In this way any imbalance in the circuit due to an unstable potentiostat, or a failing potentiostat power supply and hence unstable overpotentials, could be immediately detected since the two ammeter readings would no longer register identical values.

2.4. Procedure: Dendrite initiation and growth rate determinations

Following the insertion of the electrodes into the required zincate solution at the required temperature, the required overpotential was applied and the potentiometer and potentiostat circuits balanced as described in Section 2.3 (iii). A visual observation of the cathode spherical zinc electrode was maintained until, after a known lapse of time, dendrites were observed to have been initiated. In the growth rate experiments, the electrode assembly E was then slowly rotated until the required dendrite or dendrites were normal to the observation axis. From this point either Polaroid photographs were taken at short time intervals or a visual check was kept on the dendrite length with respect to time (for the visual measurements, an attachment eyepiece with cross wire

screen and vernier adjustments was added to the optical system). During these growth rate measurements, the total current, which was observed to increase, was also noted, again with respect to time.

The dendrite growth rate and the concurrent increase in the total current were determined as a function of overpotential in the range -75 to -200 mV, zincate ion concentration in the range 0.01 to 0.2 moles liter^{-1} and temperature in the range 25 to 50°C.

III. RESULTS

3.1. Qualitative observations on the dendrite initiation time and morphology of the deposited zinc

In the present work, the critical overpotential required for dendrite initiation was determined experimentally as lying in the range -75 to -85 mV; since there is a tendency to overestimate this critical overpotential (cf. Section 4), this experimental value is considered to be high.

Below an overpotential of -75 mV it was experimentally difficult to distinguish dendritic growth from that grown at the base electrode surface; this would suggest either (a) that there are no dendrites, or (b) that any dendrites present do not propagate at a rate significantly greater than that of the electrode surface. At overpotentials less negative than -75 mV the zinc deposit was gray to black, mossy or spongy.

Upon application of an overpotential, the zinc cathode was observed until the first definite signs of dendritic deposition were seen — this is termed the experimental initiation time. Propagation rates of individual dendrites were determined by observing the change in dendrite length as a function of time. A second initiation time is obtained when the dendrite length against time plots (Figures 9, 10, and 11, Section 3.3) are extrapolated to zero dendrite length. It is this extrapolated initiation time which is analogous to that defined by Barton and Bockris[1] in the study of silver dendrites. A third initiation time is determined from the relationship between $\log (i - i_{L,0})$ and time (where i is the current density at time t and where $i_{L,0}$ is the initial pre-dendrite current density) — this initiation time is termed τ and is determined and evaluated in Section 4.

The experimental initiation times observed were always slightly greater than those obtained by extrapolation, the error between the two becoming greater as the initiation time increased. The presence of this error would indicate that the time of dendrite initiation (as given by the extrapolated value) and the time at which the first dendrite is readily distinguishable experimentally do not coincide. Thus, as the dendrite propagation rate becomes smaller the time error becomes larger. This is in accordance with the experimental observations; the time error is the smallest for the largest propagation rates, and is the greatest when the propagation rate is low.

The character of the dendritic deposit was of the usual dendritic type, with the exception that the main axis and the primary branches appeared to be of a flat sword-like nature, especially in the fast propagation rate experiments. With respect to branching, secondary branching was rare, and tertiary branching unknown, in the present study. Figures 2 and 3 show typical dendrites from a low and fast propagation rate experiment, respectively; in both cases it can be seen that numerous dendrites have been initiated, which is unlike the behavior of silver where the occurrence of one or two dendrites only was not uncommon.[1]

At an overpotential of -200 mV it was observed that, apart from some initial dendritic growth, the deposition did not appear unlike spongy growth observed at a much lower overpotential (Figure 4). Upon lowering the overpotential to -100 mV, dendrites were quickly distinguishable after a short initiation period. The propagation rate of the dendrites at this overpotential of -100 mV was found to be identical to that found in Section 3.3, Table 4, i.e., 24μ min^{-1} at a zincate concentration of 0.1 mole $liter^{-1}$ at a temperature of 35°C. When the overpotential was increased again to -200 mV, the dendrites that had been initiated at the lower overpotential effectively ceased to propagate and were rapidly submerged in a spongy deposition. This phenomenon of initiation and submergence of dendrites upon lowering and raising the overpotential between -200 and -100 mV appeared to be reproducible and repetitive. The overpotential required for this morphological change from dendrite to

sponge-like deposition was found to lie near -160 mV, since at this overpotential the deposit observed was slightly dendritic but predominantly spongy in appearance. For this reason, qualitative observations of dendritic growth were determined in the overpotential range -85 to -140 mV. It is considered that this sponge-type deposition, observed at overpotentials more negative than -160 mV, is similar to the heavy dendritic zinc sponge reported by Stachurski[40] at overpotentials in excess of -105 mV.

3.2. Change in the total current with respect to time

In all experiments of dendritic growth the current flowing through the system at a given overpotential was observed with time. It was found (Figures 5, 7, and 8) that in all cases the current increased, from an initial value, in an exponential manner. The region of sharp current change, characteristic of exponential functions, appeared to coincide with the appearance of the first dendrites.

(a) Total current against time as a function of zincate concentration

Figure 5 shows the total current plotted against time as a function of zincate concentration, the time axis being measured relative to the moment of overpotential application. It is seen that the time required for the appearance of the first dendrites, as determined from the point at which the current changes sharply, decreases as the zincate concentration increases. In the case of 0.01 mole liter^{-1} zincate, the appearance of dendrites occurred at a time > 150 minutes.

The relationship between the initial pre-dendrite current density, calculated upon the geometric area, and the zincate concentration C_0 is shown in Figure 6. From the linear slope, assuming the validity of $i_L = \frac{nFDC_0}{\delta_0}$, the value of the term $\frac{D}{\delta_0}$ is found to be 6.8×10^{-4} cm sec^{-1}.

(b) Total current against time as a function of overpotential

Figure 7 shows total current against time as a function of overpotential, which shows that the time required for the appearance of the first dendrites decreases as the overpotential increases.

(c) Total current against time as a function of temperature

In Figure 8 is shown the increase of total current with time as a function of temperature. The time required for the appearance of the first dendrites decreases as the temperature increases. As before, the sharp increase in the current appeared to correspond to the time required for the first dendrites to appear.

3.3. The rate of dendrite propagation

(a) As a function of zincate concentration

Figure 9 shows the change in observed dendrite length with respect to time (time measured from the moment of application of the overpotential) as a function of zinc concentration. The extrapolations from the linear portions to zero dendrite length gives the initiation times as defined by Barton and Bockris.[1] In the following Table 2, where the dendrite

TABLE 2

η (mV)	T (°C)	C_0 (mole liter^{-1})	g (μ min^{-1})	i (Acm^{-2})
-100	35	0.01	2.4	0.084
		0.05	5.8	0.20
		0.07	12.3	0.43
		0.09	18.7	0.66
		0.10	24.0	0.84
		0.20	45.0	1.60

propagation rates are tabulated, it is seen that the rate of propagation increases as the concentration of zincate increases. The value of the term $\frac{dg}{dC_0}$ was obtained as 24.8 cm^4 mole^{-1} min^{-1}, where g is the propagation rate expressed in cm per minute and C_0, the zincate concentration, in moles cm^{-3}. Table 2 also tabulates the dendrite tip current density (i) calculated from the growth rate (g) assuming that no significant migration of deposited zinc from the tip occurs; thus

$$i = g \cdot \frac{nF}{V} \quad ,$$

where V is the molar volume of zinc. As will be shown in Section 4, a plot of log i against log C_0 has a significance with respect to an activation controlled deposition process — such a plot is shown in Figure 10, where

$$\frac{d \log i}{dC_0} = 1$$

(the dotted line shows a slope of 0.75 for the benefit of the discussion in Section 4).

(b) As a function of overpotential

Figure 11 shows the change in the dendrite length with respect to time as a function of overpotential. It is seen that the extrapolated initiation time decreases with increasing overpotential; the experimentally observed initiation times are in agreement with this trend. In Table 3 are tabulated the propagation rates, and the dendrite tip current density as a function of overpotential. From these results it would appear that the dendrite propagation rate increases with increasing overpotential. Figure 12(a) shows that the term $\frac{dg}{d\eta}$ has a value which increases as the overpotential increases. Figure 12(b) shows a plot of log dendrite tip current density i against η; the slope is seen to be linear where

$$\frac{d\eta}{d \log i} = 0.17 \quad .$$

(c) As a function of temperature

Figure 13 shows the change in dendrite length with respect to time as a function of temperature. It can be seen that the extrapolated initial values, in agreement with the experimentally observed values, decrease with increasing themperature.

Table 4 shows the propagation rate (g), and the calculated dendrite tip current density (i) as a function of temperature — both increase with increasing temperature; the value of

TABLE 3

C_0 (moles liter^{-1})	T (°C)	η (mV)	g (μ min^{-1})	i (A · cm^{-2})
0.10	35	-140	41.7	1.46
		-120	30.0	1.05
		-100	24.0	0.84
		- 92	21.4	0.75
		- 85	20.0	0.70

TABLE 4

η (mV)	C_0 (moles liter^{-1})	T (°C)	g (μ min^{-1})	i (A · cm^{-2})
-100	0.1	24	15.0	0.53
		35	24.0	0.84
		50	36.0	1.26

$$\frac{dg}{dT} = 8 \times 10^{-5} \text{ cm min}^{-1} \text{ deg}^{-1}$$

Figure 14 shows log dendrite tip current density i against $1/T$ which shows a linear slope of negative values where

$$\frac{d \log i}{d \frac{1}{T}} = 1.4 \times 10^{3} \text{ deg} \quad .$$

Reference is made to this value in Section 4, when an attempt is made to relate this to an activation energy term.

3.4. The influence of the dendrite propagation current upon the measured total current

In order to relate the changes in total current flowing in the system to some dendrite initiation process, it is necessary to show that the dendrite propagation current is negligible when compared to the current at the substrate surface. From the results in Table 2, the propagation rate of dendrites in a zincate concentration of 0.10 moles liter^{-1} at 35°C and an overpotential of -100 mV is equivalent to a dendrite tip current density of 840 mAcm^{-2}. From experimental observations, the dendrites so formed are approximately 10μ in width and therefore, assuming that the dendrite has a cone shape, the current to the base of the dendrite can be calculated as 0.7 μA. It is seen from Figure 5 that this level of dendrite propagation current is negligible compared to the total current observed, even allowing for as many as 30 dendrites. It can further be shown that this will be valid at all zincate concentrations,

and that it can therefore be concluded that the dendrite propagation current, and the subsequent penetration of the diffusion layer by the dendrite, contribute little to the total current observed.

IV. DISCUSSION

4.1. Diffusion-controlled deposition onto rough surfaces — initiation of dendritic growth

Perhaps the most important observation that was made at overpotentials greater than a certain critical value during predendritic and early dendritic deposition was that of the current density exponentially increasing with time; the time constant being dependent on the concentration of zincate ions in solution, on overpotential and temperature. It was realized that this phenomenon may reflect occurrences causing the subsequent appearance of dendrites, i.e., those factors responsible for dendritic growth.

A model of the predendritic developments was made as shown in Figure 15. It was assumed that (1) prior to the commencement of deposition the surface possessed a certain degree of roughness which could be described by some function (equation (1)) which need not be known precisely

$$y_0(x) = f(x) \qquad (1)$$

for the subsequent argument. It is further assumed that (2) hydrodynamic conditions in the solution are such that a concentration gradient is established whose thickness is a constant δ_0 relative to a point $y_0(0)$

representative of a flat surface. It is through this thickness of δ_0 that material must be supplied for deposition, obviously by diffusion. It is also assumed that (3) although the surface possesses some degree of roughness, described by equation (1), all values of x are such that

$$y_0(x) << \delta_0 \tag{2}$$

It was of interest to determine how the function y(x) varies with time, and this was established as follows. The rate of growth at any point at the surface is related to the current density at that point, thus

$$\frac{dy(x)}{dt} = \frac{M}{\rho nF} \tag{3}$$

where M is the atomic weight of the metal and ρ is its density. At the commencement of the deposition process there may be virtually complete diffusion control and therefore the current density i approaches $i_{L,0}$.

$$i = i_{L,0} = \frac{nFDC_0}{\delta_0} = \frac{(i_L)_0}{\delta_0} \tag{4}$$

D being the diffusion coefficient and C_0 the concentration of the depositing species in the bulk of the solution, while $(i_L)_0$ is the limiting current density at unit diffusion layer thickness. As surface deposition proceeds, at some points where the current density is high, i.e., roughness 'peaks,' the current density may come partially under activation control. Hence, treatment in a general form using an equation of the type

$$i = i_0 \{ \frac{i_L - i}{i_L} \cdot i_{a,c} - i_{a,a} \} \tag{5}$$

where

$$i_{a,c} = \exp\left(-\frac{\alpha_c F}{RT} \cdot \eta\right) \tag{6}$$

and

$$i_{a,a} = \exp\left(\frac{\alpha_a F}{RT} \cdot \eta\right) \tag{7}$$

one obtains explicitly

$$i = \frac{i_L(i_{a,c} - i_{a,a})}{\frac{i_L}{i_0} + i_{a,c}} \tag{8}$$

Now, taking equation (4) and representing δ as a function of x and t

$$i_L = \frac{(i_L)_0}{\delta_{x,t}} \tag{9}$$

and since the point representative of the flat surface $y(0)$ is advancing with time t relative to $y_0(0)$ due to deposition, the position of the outer boundary of the diffusion layer is given by $\delta_0 + y_0$, again relative to the original flat surface $y_0(0)$. Following this, the value of δ as a function of time t and position $y(x)$ is given by

$$\delta_{(t,x)} = \delta_0 + y(0) - y(x) \tag{10}$$

Introducing (10) into equations (8), (9), and (3) and rearranging, the following equation is obtained

$$\frac{dy(x)}{dt} = \frac{M}{\rho n F} \frac{(i_L)_0\left(1 - \frac{i_{a,a}}{i_{a,c}}\right)}{\frac{(i_L)_0}{i_0 \cdot i_{a,c}} + \delta_0 + y(0) - y(x)} \tag{11}$$

Since the interest is in the propagation at point x relative to point 0, the variable given in equation (12) is introduced

$$y = y(x) - y(0) \tag{12}$$

where

$$\frac{dy}{dt} = \frac{dy(x)}{dt} - \frac{dy(0)}{dt} \tag{13}$$

From (11) it follows that

$$\frac{dy(0)}{dt} = \frac{M}{\rho n F} \cdot \frac{(i_L)_0 (1 - \frac{i_{a,a}}{i_{a,c}})}{\frac{(i_L)_0}{i_0 \cdot i_{a,c}} + \delta_0 + y(0) - y(x)} =$$

$$= \frac{M}{\rho n F} \frac{(i_L)_0 (1 - \frac{i_{a,a}}{i_{a,c}})}{\frac{(i_L)_0}{i_0 \cdot i_{a,c}} + \delta_0} \tag{14}$$

Introducing (14) into (13) and replacing $\frac{dy(x)}{dt}$ in (11), one obtains

$$\frac{dy}{dt} = \frac{M}{\rho n F} (i_L)_0 (1 - \frac{i_{a,a}}{i_{a,c}}) \left[\frac{1}{\frac{(i_L)_0}{i_0 \cdot i_{a,c}} + \delta_0 - y} - \frac{1}{\frac{(i_L)_0}{i_0 \cdot i_{a,c}} + \delta_0} \right] \tag{15}$$

or, upon rearranging,

$$\frac{dy}{dt} = \frac{M}{\rho n F} \frac{(1 - \frac{i_{a,a}}{i_{a,c}})(i_L)_0}{\frac{(i_L)_0}{i_0 \cdot i_{a,c}} + \delta_0} \left[\frac{y}{\{\frac{(i_L)_0}{i_0 \cdot i_{a,c}} + \delta_0\} - y} \right] = \frac{A}{B} [\frac{y}{B - y}] \tag{16}$$

Integration of (16) between y and y_0 produces

$$B \ln y - y = \frac{A}{B} t + B \ln y_0 - y_0 \tag{17}$$

At the early stage of initiation $y << \delta_0$ and hence $y << B$, thus it can be neglected in (16). Integrating (16) with this approximation reduces (17) to

$$\ln y = \frac{A}{B^2} t + \ln y_0 \tag{18}$$

or

$$y = y_0 \exp\left\{\left[\frac{M}{\rho nF}\left(1 - \frac{i_{a,a}}{i_{a,c}}\right)\frac{(i_L)_0}{\left(\frac{(i_L)_0}{i_0 \cdot i_{a,c}} + \delta_0\right)^2}\right] t\right\} \tag{19}$$

Since $y(0) = f(x)$ — equation (1) — this means that the function y will reproduce the substrate with a factor <u>exponentially increasing with time</u>, i.e., the original surface roughness tends to become amplified and because of the exponential dependence with time, it "suddenly" becomes visible. Figure 16 represents an idealized model ($y_0 = a \pm bx$) at different constant time intervals, with the values of the relative time $\frac{t}{\tau} = 1, 2, 3, 4, \ldots$ where the time constant τ is defined as

$$\tau = \frac{\left\{\frac{(i_L)_0}{i_0 \cdot i_{a,c}} + \delta_0\right\}^2}{\frac{M}{\rho nF}\left(1 - \frac{i_{a,a}}{i_{a,c}}\right)(i_L)_0} \tag{20}$$

This model appears to explain the cause of the dendrite initiation; any elevation at the original surface obviously will tend to amplify and develop the original crystallite into a protrustion.

Equation (19) is, however, only an approximate solution, and can only be assumed to hold so long as the protrusion is small compared to

the diffusion layer thickness. As soon as the protrusion size is comparable to the diffusion layer thickness, the diffusion layer should start bending around the tip; and a new law should govern further deposition, i.e., that of the dendrite propagation. Equation (19) reveals also the significance of the so-called initiation or induction period. Due to the exponential nature of the function, the marked change from a slowly growing invisible protrusion to a rapidly growing visible dendrite should occur at time τ, as defined in equation (20).

In systems of large enough i_0 values and at high overpotentials at which $i_{a,a} << i_{a,c}$, equation (20) reduces to:

$$\tau = \frac{\delta_0^2}{(i_L)_0} = \frac{\delta_0^2}{nFDC_0} \qquad (21)$$

It is seen that τ depends on the inverse of the bulk ion concentration of the depositing species and on the inverse of the diffusion coefficient. This latter term, being temperature dependent in the known fashion, will be related to τ in that τ should decrease exponentially with temperature increase. Both conclusions are in qualitative accordance with the observed facts.

In systems with relatively low i_0 values, the term $(i_L)_0 / i_0 \cdot i_{a,c}$ becomes comparable to δ_0 and a potential dependence of τ is then to be expected. As the overpotential increases, $(i_L)_0 / i_0 \cdot i_{a,c}$ should decrease as should the value of τ. This is also in accordance with experimental observations.

Finally, the time τ represents the time at which y/y_0 attains the value of 2.72 (cf. equation (19)).

Experimental conclusions about the initiation time, as the time in which the dendrite becomes visible, are based upon an absolute value of y; hence, the larger the y_0, i.e., the larger the original surface roughness, the shorter should be the initiation time. This is shown to be the case in Figure 17 where the initiation time for a pre-roughened electrode is considerably less than that for a smooth plated zinc electrode.

4.2. The time dependence of the current density during deposition onto a rough surface

To get a quantitative estimate of the above model of dendrite initiation, the consequences for the measured apparent current density per unit of geometric surface area must be considered.

The current density at any point can be obtained from equation (3). Differentiating equation (19) and introducing the result into (13) and combining with (14) one obtains the following expression:

$$\frac{dy(x)}{dt} = \frac{1}{\tau}\left[y_0 \exp\left(\frac{t}{\tau}\right) + \left(\frac{(i_L)_0}{i_0 \cdot i_{a,c}} + \delta_0\right)\right] \qquad (22)$$

If this expression is then placed into (3), upon rearranging, the current density at each point x is given by:

$$i = \frac{(i_L)_0}{\left(\frac{(i_L)_0}{i_0 \cdot i_{a,a}} + \delta_0\right)} \left(1 - \frac{i_{a,a}}{i_{a,c}}\right) \left[1 + \frac{y_0}{\left(\frac{(i_L)_0}{i_0 \cdot i_{a,c}} + \delta_0\right)} \exp\left(\frac{t}{\tau}\right)\right] \qquad (23)$$

which is larger than the limiting current at the flat surface by the exponential term within the squared brackets.

In order to attain the current per unit geometric surface area of the electrode as the average current density, one should make a two-dimensional integration of equation (23) over all values of x and z up to 1 cm, and divide the result by xz. This would result in another constant in the exponential term of the equation. Since

$$i_{L,0} = \frac{(i_L)_0}{\frac{(i_L)_0}{i_0 \cdot i_{a,c}} + \delta_0} \left(1 - \frac{i_{a,a}}{i_{a,c}}\right) \qquad (24)$$

the current density per unit geometrical surface area can be given as

$$i = i_{L,0} \left[1 + \frac{y_0'}{\frac{(i_L)_0}{i_0 \cdot i_{a,c}} + \delta_0} \exp\left(\frac{t}{\tau}\right)\right] \qquad (25)$$

and this should be equal to the experimentally measured c.d. at the electrode as a function of time.

An interesting point which emerges from an analysis of equation (25) is that the exponential increase in current with time, as well as the growth of protrusions causing it, do not necessarily require complete, or even predominant, diffusion control of the deposition. In the case of very low i_0 values or high overpotentials, or both, it may be that

$$\frac{(i_L)_0}{i_0 \cdot i_{a,c}} << \delta_0 \quad ,$$

so in this case the existence of a diffusion layer obviously loses its significance in the pre-exponential factor, and $i_{L,0}$ becomes a purely activation controlled current density (cf. equation (24)). However, the diffusion coefficient is still involved, both in the pre-exponential and exponential terms, indicating that the basic reason for the phenomenon is still the difference in the rates of transport to different points upon the electrode surface. In conclusion, one may say that the increase in the surface roughness, and thus the initiation of dendritic growth, does not necessarily require diffusion control of the rate of deposition.

In order to verify the validity of equation (25), rearrangement of which produces

$$\log (i - i_{L,0}) = \frac{t}{2.3\tau} + \log \frac{i_L y_0'}{\frac{(i_L)_0}{i_0 \cdot i_{a,c}} + \delta_0} \quad , \qquad (26)$$

the values of τ were extracted and analyzed for their dependence on (i) concentration of depositing species, (ii) overpotential, and (iii) temperature. Experimental plots of $\log (i - i_{L,0})$, where the value of $i_{L,0}$ was taken as the initial current density, against time are shown in Figures 18, 19, and 20, where the changing parameters were concentration, overpotential, and temperature, respectively, other alternative parameters being held constant. It can be seen that reasonable linear plots are

obtained, and the values of τ extracted from the slopes are shown in Table 5.

In order to analyze the concentration dependence of τ, equation (20) can be rewritten as

$$\tau = \frac{\left(\frac{nFD}{i_0^0 \cdot i_{a,c}} \cdot \frac{C_0}{C_0}\right)^2}{\frac{M}{\rho nF}\left(1 - \frac{i_{a,a}}{i_{a,c}}\right) nFDC_0} \qquad (27)$$

where i_0^0 is the standard exchange current density and the exponent $(1 - \frac{\beta}{2})$ corresponds to the assumed zincate discharge mechanism. In systems with high i_0 values, under complete diffusion control, the first term in the numerator would be negligible compared to the second, and the result would be a simple hyperbolic relationship between τ and C_0. Since in the present case the current is, on the one side, dependent on stirring and, on the other, dependent on overpotential, it is clear that the control is a mixed one and no term in (27) can be neglected. Hence (27) is rearranged to produce equation (28):

$$(\tau C_0)^{\frac{1}{2}} = \frac{nFD^{\frac{1}{2}}\rho^{\frac{1}{2}}}{M^{\frac{1}{2}} i_0^0 i_{a,c}} \cdot C_0^{\frac{\beta}{2}} + \frac{\delta_0 \rho^{\frac{1}{2}}}{M^{\frac{1}{2}} D^{\frac{1}{2}}} \qquad (28)$$

so therefore if $\frac{\beta}{2} = \frac{1}{4}$, a linear dependence of $(\tau C_0)^{\frac{1}{2}}$ on $C_0^{\frac{1}{4}}$ would be expected from the experimental results. Such a relationship is seen to exist in Figure 21. The theoretical slope can be calculated for any value of overpotential if a value for i_0^0 can be estimated. Taking the value of

TABLE 5

Time constants τ as determined from equation (26)

	Concentration C_0 of zincate ion mole cm^{-3}	Temperature °C	Overpotential η (mV)	Time constant τ
A	0.1×10^{-3}	35	-100	545
	0.09			558
	0.07			681
	0.05			866
B	0.1×10^{-3}	24	-100	774
		35		545
		50		375
C	0.1×10^{-3}	35	- 85	1055
			- 92	966
			-100	545
			-120	432
			-140	365

$i_0 = 10^{-1}\,A\,cm^{-2}$ at a zincate concentration of 10^{-4} mole cm^{-3} as reported by Farr and Hampson,[41] then

$$i_0^0 = \frac{i_0}{C_0^{(1-\frac{\beta}{2})}} = \frac{10^{-1}}{10^{-3}} = 10^2\,A\ \text{mole}^{-\frac{3}{4}}\ cm^{\frac{1}{4}} \qquad (29)$$

Introducing (29) into (28) and using $n = 2$, $D = 1.5 \times 10^{-5}\ cm^2\ sec^{-1}$, $\rho = 7.1$ gms cm^{-3}, and $i_{a,c} = 6.82$ for $\eta = -100$ mV, the slope of the straight line in Figure 21 should be about 0.5 $sec^{\frac{1}{2}}$ $mole^{\frac{1}{4}}$ $cm^{-\frac{3}{4}}$. If the value of i_0 is taken as 12 $mA\,cm^{-2}$, as obtained in dendrite growth experiments (see later), at a zincate concentration of 10^{-5} moles cm^{-3}, then a calculation comparable to the one above produces a slope value of 0.6 $sec^{\frac{1}{2}}$ $mole^{\frac{1}{4}}$ $cm^{-\frac{3}{4}}$. Experimentally a slope of 1.5 is obtained; considering that this slope represents a second derivative of the experimental results, the agreement within an order of magnitude can be considered as satisfactory.

The value of δ_0, as calculated from the intercept of the slope at the $(\tau C_0)^{\frac{1}{2}}$ axis, i.e., $(\tau C_0)^{\frac{1}{2}} = 8 \times 10^{-2}$, is found to be about 10^{-3} cm, a value which is not too unexpected.

Referring again to equation (27), the two terms in the numerator can now be calculated from the slope and the intercept of Figure 21. Thus:

$$\frac{nFD}{i_0^0 \cdot i_{a,c}} C_0^{\frac{1}{4}} = 2.3 \times 10^{-3}\,cm$$

and

$$\delta_0 = 10^{-3}\ cm \quad ,$$

and therefore it is clear that the assumption of a mixed diffusion and activation control of the deposition process is confirmed, i.e., neither term can be neglected when compared to the other.

In order to assess the theoretical temperature dependence of τ, equation (20) can be written as

$$\tau^{\frac{1}{2}} = \frac{P \cdot \frac{D}{i_0^0} + \delta_0}{Q D^{\frac{1}{2}}} = K \cdot \frac{D^{\frac{1}{2}}}{i_0^0} + K' D^{-\frac{1}{2}} \tag{30}$$

where the constants $P, Q, K,$ and K' are temperature independent. Assuming an Arrhenius type temperature dependence for D and i_0^0, it is possible to write

$$\tau^{\frac{1}{2}} = \mathcal{H} \exp\left[\frac{(E_a - \frac{1}{2}E_d)}{RT}\right] + \mathcal{H}' \exp\left[\frac{(\frac{1}{2}E_d)}{RT}\right] \tag{31}$$

where E_a and E_d are the activation energies for diffusion and the discharge process, respectively. Although it is not possible to produce a simple result for the derivative

$$\frac{d \log \tau}{d(\frac{1}{T})}$$

from equation (31), it is seen that in two limiting situations, where one term can be neglected when compared to the other term, the two derivatives would be the following:

$$\frac{d \log \tau}{d(\frac{1}{T})} = \frac{(2E_a - E_d)}{2 \cdot 3R} \tag{32}$$

and

$$\frac{d \log \tau}{d(\frac{1}{T})} = \frac{E_d}{2 \cdot 3R} \tag{33}$$

In either case a straight line with a positive slope should be obtained for a $\log \tau$ against $\frac{1}{T}$ plot. Experimentally it is seen that this is so — Figure 22. A value for the activation energy of 5.5 kcal $mole^{-1}$ was obtained from the slope; however, it is difficult to give this value any physical significance. A similar temperature dependence is exhibited by the initial predendrite current density at the electrode as is seen in Figure 23; in this instance an activation energy of 4.1 kcal $mole^{-1}$ was obtained from the slope. Although equation (23) cannot be simply solved for

$$\frac{d \log i}{d(\frac{1}{T})} ,$$

if, as a first approximation, a complete diffusion control is assumed, equation (23) can be written as

$$i = \frac{nFDC_0}{\delta_0} [1 + \frac{y_0}{\delta_0^2}] \tag{34}$$

Referring again to the Arrhenius type of equation where

$$i = A \exp (-\frac{E_d}{RT}) \tag{35}$$

i.e.,

$$\frac{d \log i}{d(\frac{1}{T})} = \frac{-E_d}{2 \cdot 3R} \tag{36}$$

The evaluation of the log i against $(\frac{1}{T})$ produces, as mentioned above, a value for the activation energy of diffusion of about 4 kcal $mole^{-1}$, which is of the order expected for a diffusion controlled process, and comparable to those values reported elsewhere.[42]

The overpotential dependence of the time constant τ can be obtained from equation (20); at high overpotentials where

$$(1 - \frac{i_{a,a}}{i_{a,c}}) \rightarrow 1 \quad ,$$

the following equation can be obtained:

$$\tau^{\frac{1}{2}} = \frac{nFD^{\frac{1}{2}}\rho^{\frac{1}{2}}C_0^{\frac{1}{2}}}{M^{\frac{1}{2}} i_0} \exp(\frac{\beta F}{RT} \cdot \eta) + \frac{\delta_0 \rho^{\frac{1}{2}}}{(MDC_0)^{\frac{1}{2}}} \qquad (37)$$

The results from Table 5 (part C), at the concentration of zincate 0.1 mole $liter^{-1}$, are plotted as $\tau^{\frac{1}{2}}$ against

$$\exp(\frac{\beta F}{RT} \cdot \eta)$$

in Figure 24; the solid line in Figure 24 is the calculated theoretical slope value of 27. It is seen that the results are not inconsistent with the theoretical trend expected. The value obtained for δ_0, from the intercept at $\tau^{\frac{1}{2}} = 0$, was calculated as 2.9×10^{-3} cm, i.e., of the same order as that obtained from the concentration dependence calculations. The theoretical slope value of 27 is obtained when $i_0 = 100$ mA cm^{-2}, consequently if i_0 is lower the slope will be larger. The dotted line in Figure 24 was calculated assuming that $i_0 = 23$ mA cm^{-2}, and it is seen that perhaps this line fits the experimental points more closely than the

solid line. From the intercept, at

$$\exp\left(\frac{\beta F}{RT} \cdot \eta\right) = 0 \quad ,$$

the dotted line produces a value of $\delta_0 = 10^{-3}$ cm, which is in better agreement with the δ_0 value obtained earlier.

4.3. Rate of dendrite propagation

The concept of spherical diffusion to the dendrite tip developed by Barton and Bockris, in which the propagation rate of the tip was controlled both by increased diffusion and by the surface energy of the growing tip (these two factors being in opposition produced an optimum tip radius for maximum propagation rate), were proved sufficiently correct to justify further development of the theory of dendrite growth on these concepts. However, it was necessary when accounting, in a quantitative manner, for the phenomena observed at high overpotentials to recognize that the linearization of the kinetic equations was no longer justified. It also had to be realized that the mechanisms of discharge of silver and zinc ions is rather different and that this may have significant consequences for the quantitative aspects of the theory. It is assumed that the deposition of zinc from zincate solutions follows the two-step charge transfer reactions given below, with the first step rate-determining.

$$Zn(OH)_4^{=} + e^- \rightarrow Zn(OH)_2^{-} + 2\,OH^-$$

$$Zn(OH)_2^{-} + e^- \rightleftharpoons Zn + 2\,OH^-$$

Since the second step is in equilibrium, any change in the standard free energy, i.e., activity of the metal, should produce a corresponding change in the concentration of the intermediate species $Zn(OH)_2^-$ and hence in the rate of the reverse reaction. Such a change in the activity of the surface atoms of zinc will occur as the radius of a dendrite or protrusion tip decreases; the degree of this change with respect to a flat surface will be given by the surface energy term $2\gamma V/r$, where γ is the surface tension between metal and solution. The known kinetic equation for the two-step single electron exchange reactions can be modified to take into account both the change in concentration of zincate ions at the surface, and the change in the activity of the metallic zinc, i.e.,

$$i = i_0 \left\{ \frac{C_{Zn(OH)_4^=}}{(C_{Zn(OH)_4^=})_0} \exp\left[-\frac{\beta F}{RT} \cdot \eta \right] - \frac{a_{Zn}}{(a_{Zn})_0} \exp\left[\frac{(1+\beta)F}{RT} \cdot \eta \right] \right\} \tag{38}$$

Now

$$\frac{C_{Zn(OH)_4^=}}{(C_{Zn(OH)_4^=})_0} = \frac{i_{L,S} - i}{i_{L,S}} \tag{39}$$

where $i_{L,S}$ is now the spherical diffusion limiting current and is given by

$$i_{L,S} = \frac{nFDC_0}{r} \quad , \tag{40}$$

where r is the radius of the dendrite tip, and

$$\frac{a_{Zn}}{(a_{Zn})_0} = \exp\left(\frac{2\gamma V}{RTr}\right) \quad . \tag{41}$$

Introducing (39) and (41) into (38), and solving for i, one obtains equation (42).

$$i = \frac{i_0 \left\{ \exp\left[-\frac{\beta F}{RT} \cdot \eta \right] - \exp\left[\frac{(1+\beta)F}{RT} \cdot \eta \right] \exp\left[\frac{2\gamma V}{RTr} \right] \right\}}{1 + i_0 \exp\left[\frac{\beta F}{RT} \cdot \eta \right] \frac{r}{nF DC_0}} \tag{42}$$

Defining

$$i_{a,c} = \exp\left[-\frac{\beta F}{RT} \cdot \eta \right] \tag{43}$$

and

$$i_{a,a} = \exp\left[\frac{(1+\beta)F}{RT} \cdot \eta \right] \tag{44}$$

as the cathodic and anodic activation controlled current densities at $i_0 = 1$ and also normalizing the tip radius so that the normalized tip radius (r_n) is given by

$$r_n = \frac{r}{\frac{2\gamma V}{RT}} \tag{45}$$

With equations (43), (44), and (45) introduced into equation (42) and then rearranging, the following equation (46) is obtained which is an expression for the current density at

$$\frac{i}{K} = i_n = \frac{i_{a,c} - i_{a,a} \exp\left[\frac{1}{r_n} \right]}{\frac{K}{i_0} + i_{a,c} r_n} \tag{46}$$

the dendrite tip normalized by a constant K where

$$K = \frac{RTnF DC_0}{2\gamma V} \tag{47}$$

It is seen that the rate of propagation of the dendrite tip is a complex function of the tip radius. At very low values of this radius, when the second term in the denominator becomes negligible, the value of i_n instead of tending to a constant value characteristic of pure activation control, i.e., $i_0 (i_{a,c} - i_{a,a})$ will decrease to zero within a very small range of r_n values due to exponential effect of the tip radius upon the second term in the numerator. At large values of r_n, when the exponential term is negligible, the term in the denominator representing the inverse of a normalized exchange current density becomes of crucial importance. For example, when i_0 is large, equation (46) gives the maximum attainable current densities as a direct inverse of the normalized tip radius, or a straight line with a slope of -1 in the log-log system. However, at small values of the exchange current density and at low overpotentials ($i_{a,c}$ small), the term $i_{a,c} r_n$ tends to become negligible when compared to K/i_0; if the range of r_n values required to make this assumption is such that

$$\exp\left[\frac{1}{r_n}\right]$$

is virtually equal to unity, then a plateau will be exhibited in the i_n against r_n plot, whose values will be given by

$$i = i_0 (i_{a,c} - i_{a,a}) \tag{48}$$

This plateau represents the maximum attainable rate of growth, for the given i_0 and overpotential, when the supply of ions by spherical diffusion to the dendrite tip is of sufficient magnitude so that the deposition process is entirely activation controlled. It is seen that for a given overpotential,

the i_0 values can be determined if the dendrite growth rate (representative of i) can be experimentally determined. For example, at a zincate concentration of 0.01 moles liter^{-1}, 35°C and at an overpotential of -100 mV, the current density at the tip calculated from the observed growth rate was found to be 84 mA cm^{-2} (the calculation assumes that the zinc depositing at the dendrite tip does not diffuse to any significant extent away from the tip). The i_0 value was found to be 12 mA cm^{-2}, which is in fair agreement with the values reported in the literature. Using this value of i_0, a set of curves were calculated using equation (46) for several values of overpotentials. The results are shown in Figure 25. The horizontal line in Figure 25 is the normalized value of the limiting current density for diffusion to a flat surface $(i_{L,\ell})_n$ calculated using the value of $\delta_0 = 10^{-3}$ cm obtained earlier. It can be seen that that $i_n - r_n$ curve for - 50 mV, is below, whilst that of -75 mV is above the $(i_{L,\ell})_n$ value. This led to the conclusion that this fact is determining the critical overpotential, i.e., dendrites will appear when the overpotential is such that the $i_n - r_n$ curve crosses over the linear diffusion limiting current density line for any value of r.

In those cases where equation (46) shows a plateau i_n value over a range of r_n values, the value of the plateau i_n can be solved explicitly for the value of the critical overpotential. Thus,

$$i_{L,\ell} = \frac{nFDC_0}{\delta_0} = i = i_0 (i_{a,c} - i_{a,a}) \qquad (49)$$

and for overpotentials at which $i_{a,a} \ll i_{a,c}$,

$$-\eta_c = \frac{RT}{\beta F} \ln \left[\frac{i_{L,\ell}}{i_0}\right] = \frac{RT}{\beta F} \ln \left[\frac{nFD}{\delta_0} \cdot \frac{C_0}{\delta_0}\right] \tag{50}$$

From this approximate calculation a value for the critical overpotential η_c of about -50 mV was found for zinc deposition. From Figure 25 this value is seen to be in good agreement with the overpotential required for the $i_n - r_n$ curve to cross the $(i_{L,\ell})_n$ line.

In order to check on the general nature of these conclusions in the case of zinc, a derivation, analogous to the above, of the complete kinetic equation for the case of silver deposition was made. In the case of silver, the increase in the surface energy with decreasing tip radius directly influences the energy barrier, and hence an exponential term is found with the cathodic current density term in the equation (51) which is analogous to equation (46):

$$i_n = \frac{i_{a,c} \exp\left[-\frac{1}{r_n}\right] - i_{a,a} \exp\left[\frac{1}{r_n}\right]}{\frac{K}{i_0} + i_{a,c} \exp\left[-\frac{1}{r_n}\right]} \tag{51}$$

$i_n - r_n$ curves for silver deposition analogous to Figure 25 are shown in Figure 26, assuming $i_0 = 50\ A\,cm^{-2}$, $\gamma = 2000$ ergs cm^{-2}, $C_0 = 5 \times 10^{-4}$ mole cm^{-3}, $D = 1.4 \times 10^{-5}\ cm^2\ sec^{-1}$, and $T = 581°K$ (these values are due to the Barton and Bockris work upon silver deposition from molten salts). It is seen that the horizontal line representing the linear diffusion limiting current density $(i_{L,\ell})_n$ places the critical overpotential value between

1 and 2 mV, which is in remarkable agreement with the value of 3 mV reported by Barton and Bockris.[1] In practice, there will be a tendency to overestimate the critical overpotential in experimental observations, due to the fact that the difference in the growth rates between the dendrite tip and the flat surface should be pronounced in order to make dendrite observation possible.

One very important conclusion arises from the comparison of Figures 25 and 26. It is seen that in the case of the silver deposition mechanism, with its accompanying high i_0 value, the $i_n - r_n$ curves have a parabolic nature where the maximum occurs over a relatively narrow range of tip radii — at which point the current densities are many orders of magnitude larger than $i_{L,\ell}$. However, in the case of zinc deposition, with its low accompanying i_0 value, broad plateaux and much lower current densities, relative to $i_{L,\ell}$, are observed. If one considers that the probability of finding a crystallite in a certain region depends on the width of that region, then this could explain the experimentally observed difference in the character of the dendritic growth on the two metals, i.e., the appearance of very few fast growing dendrites in the case of silver, and many more slowly growing dendrites in the case of zinc.

Finally, the Figure 27 shows that this phenomenon is due more to the effect of i_0 than to differences in the mechanism of deposition. It can be seen that by employing equation (46) for the zinc deposition

mechanism and increasing the i_0 values, at a certain overpotential, the tendency towards a parabolic sharp maximum increases, as i_0 increases. It is also seen from Figure 27 that dendrites will initiate at an overpotential of -100 mV when the i_0 value approaches 10 mA cm^{-2}.

As for the concentration and potential dependence of the rate of dendrite growth, it is evident that in the case of low i_0 systems where the greatest number of dendrites grow at the plateau rate, these relationships will be those of any activation-controlled current density, i.e.,

$$\left(\frac{d \ln i}{d \ln C_0}\right)_{\eta, T} = \left(1 - \frac{\beta}{2}\right) \approx 0.75 \tag{52}$$

$$\left(\frac{d \ln i}{d\eta}\right)_{T, C_0, \eta < 0.04} = -\frac{\beta F}{RT} \tag{53}$$

and

$$\left(\frac{d \ln i}{d\left(\frac{1}{T}\right)}\right)_{C_0, \eta} = -\frac{E_a}{RT} \tag{54}$$

Plots of $\ln i$, as calculated from the growth rate measurements, against $\ln C_0$ and $\ln i$ against $\left(\frac{1}{T}\right)$ are shown in Figures 10 and 14. It is seen that the concentration dependence follows the slope of 0.75, within the limits of experimental error, fairly closely. The temperature dependence is again of the Arrhenius type and renders an apparent activation energy of 6.4 kcal mole^{-1}, which is similar to that obtained from the $\tau - \left(\frac{1}{T}\right)$ relationship, i.e., 5.5 kcal mole^{-1}.

The log i against η relationship as per equation (53) can be seen in Figure 12(b). The slope is seen to be linear and possess a value of

$$\frac{d \log i}{d\eta} = 5.9$$

which is in fair agreement with the theoretical value, assuming $\beta = 0.5$, of 8.21. Qualitatively it would appear that the deposition of zinc at the dendrite tip is under activation control, where, due to spherical diffusion to the tip, the flux of material to the tip is sufficiently great to produce an activation controlled deposition.

Finally, the transition at -160 mV from a definite dendritic deposition, in which growth measurements could be made, to the deposition of what appears to be a heavy dendritic sponge, is difficult to understand. From Figure 25 it was seen that as the overpotential increases the tendency to a single dendrite situation should increase, and consequently the reverse of the experimental observations might have been expected. It is suggested that the deposition of zinc by a secondary process may be occurring, involving either H_2 evolution or possibly foreign cation deposition,[19,20] e.g., in this case, K.

Summarizing, this work appears to have provided the answers to several basic questions as to the phenomenon of dendritic growth, and these are: —

(a) What is the mechanism of the initiation of dendritic deposition,

(b) What is the significance of the induction or initiation period,

(c) What is the significance of the critical overpotential, and

(d) Why certain metals produce fast growth of individual dendrites

while other metals produce simultaneous appearance of many dendrites of relatively slow growth rate.

In conclusion, one may say that conditions of complete diffusion control of the deposition process, attainable in systems of high i_0 values, are ideal for dendritic growth. In such systems, the growth of individual crystallites, whose diameter is such that its growth rate is many orders of magnitude higher than the growth rate of other sized crystallites, is predominant.

However, even under conditions of mixed diffusion and activation control, i.e., systems of intermediate i_0 values, dendrites can appear, but the range of diameter values is much broader than in the high i_0 systems, consequently a much larger number of crystallites grow simultaneously at comparable rates.

Finally, as activation control prevails, as in systems of low i_0 values, or at high concentration of depositing species, the range of diameter values of the growing crystallites is now so wide that it practically encompasses all crystallite sizes existing at a metal surface, and hence the surface exhibits virtually a compact growth. The attainment of the large current densities required to promote diffusion control, of all but a certain narrow size range of crystallites, would require such high overpotentials that secondary processes are certain to develop simultaneously, resulting in the absence of normal growth.

4.4. Concluding remarks

It would appear that, for the first time, we have a model for dendritic growth, based upon simple electrodic parameters, which can be applied to all metals.

It has been shown that, apart from the Kelvinian nature of the dendritic tip which forms an integral part of the theory, the most important electrodic parameter is the exchange current density i_0 for the metal deposition process. Due to the inverse relationship between i_0 and the type of dendritic deposit obtained, the following can be proposed as general rules of dendritic deposition:

Metals with high i_0 values ($> 5\ A\,cm^{-2}$ — low η_c (< 10 mV) with the formation of a small number of rapidly growing dendrites.

Metals with low i_0 values ($< 1\ A\,cm^{-2}$) — high η_c (> 50 mV) with the formation of a large number of slowly growing dendrites.

It should be emphasized here that although the overpotential appears to be the critical parameter in the initiation of dendrites, the critical overpotential is in fact only important in that it defines the critical activation density. Consider the equation

$$i_{crit} = i_{L,\ell} = \frac{nFDC_0}{\delta_0} = i_0 (i_{a,c} - i_{a,a})$$

Dendrites will be initiated when the tip current densities $i > i_{crit}$, i.e., when a purely activation controlled current density for a given overpotential η

exceeds the current density obtainable at the flat surface under linear diffusion control $i_{L,\ell}$.

Hence to avoid dendritic growth at zinc electrodes on charging, the charging current density should be such as to produce overpotentials smaller than η_c, which then in turn produces activation controlled current densities which are smaller than i_{crit}. Therefore the following equations can be written:

$i < i_{L,\ell}$	predendritic region
$i_{crit} = i_{L,\ell} = i_0 \frac{\beta F}{RT} \eta_c$	dendrite initiation
$i > i_{L,\ell}$	dendrites abundant

It can be seen that any factor which increases $i_{L,\ell}$, without an accompanying increase in i, will increase the range of operating current density in the predendritic region, i.e., increasing the concentration of the depositing species or decreasing δ_0 by stirring, etc.

If in the D.C. charging cycle of zinc electrodes, the current densities used are always greater than $i_{L,\ell}$, then dendrites will invariably be produced after a certain initiation time. What can be done to increase this initiation time to a time in excess of the charging time?

The initiation time increases as i_0 is decreased, as temperature is decreased, and as the concentration of the depositing species is decreased (note the reverse trend with concentration when $i > i_{L,\ell}$).

The initiation of the dendritic deposits occurs at a point where $i_{L,\ell} = i_0 \cdot i_{a,c} = i_c$. If dendrite initiation cannot be prevented, i.e, those cases where $i > i_{L,\ell}$ and charge times in excess of the initiation time, then what can be done to reduce the dendrite propagation rate? Decreasing the i_0 value has been seen to produce a second effect apart from the influence upon η_c, in that as i_0 decreases the range of dendrite tip radii at which dendrite propagation can occur increases. Effectively, this means that when exceeding $i_{L,\ell}$ a mass of dendrites begin propagating at approximately equal rates, and, although loose, the deposit has an even appearance. No individual dendrites are observed, and the propagation rate of such a dendrite front is lower, at one and the same current, than that of individual dendrites.

In conclusion, i_0 appears to be of overwhelming importance in that it can not only raise η_c, but also produces a situation where fast propagating single dendrites are an unfavorable event.

Basically, the answer is a matter of three choices:

(a) Increase $i_{L,\ell}$ so that $i \ll i_{L,\ell}$.

(b) If (a) is not possible, produce a situation which has a long dendrite initiation time.

(c) If neither (a) nor (b) is possible, produce a situation where the dendrite propagation rate is slow; thereby, even if dendrites are formed, separator penetration will be reduced.

REFERENCES

1. Barton, J.L., and Bockris, J.O'M., Proc. Roy. Soc. London, A268, 485 (1962).

2. Reddy, T.B. J. Electrochem. Soc. 113, 117 (1966).

3. Dillamore, I.L., Smallman, R.E., and Roberts, W.T. Phil. Mag. 9, 517 (1964).

4. Dobson, P.S., and Smallman, R.E. Proc. Roy. Soc. London, A293, 423 (1966).

5. Hamilton, D.R. Electrochim. Acta 8, 731 (1963).

6. Titov, P.S., and Paleolog, E.N. Yibileĭnyĭ Sbornik Nauch, Trudov Inst. Tsventykh Metal i. Zolata 9, 602 (1940); Chem. Abstr. 37, 5660.

7. Kudryavtsev, N.T., and Atansayants, A.G. Zhur. Fiz. Khim. 29, 1227 (1955).

8. Oxley, J.E., and Fleischman, C.W. Leesona Moos Corp., NASA Quart. Rept. No. 3 (1966).

9. Zholudev, M.D., and Stender, V.V. Zhur. Poiklad. Khim. 31, 1036 (1958).

10. Kudryavtsev, N.T., and Atansayants, A.G. Trudy Moskov Khim. Tekhel. Inst. im. D.I. Mendeleeva 22, 143 (1956); Chem, Abstr. 52, 926e.

11. YuBek, R., and Kudryavtsev, N.T. Izvest. Vysshikh. Vcheb. Zavedenił, Khim. i. Khim, Tekhol. 3, 898 (1960); Chem. Abstr. 55, 8115i.

12. Romanov, V.V. Zhur. Priklad. Khim. 36, 1057 (1963),

13. Krivtsov, A.K. Trudy Ivanovsk. Khim. Tekhnol. Inst, 7, 87 (1958); Chem. Abstr. 54, 20572e.

14. Romanov, V.V, Zhur. Pricklad. Khim. 36, 1050 (1963).

15. Ibl, N. Adv. in Electrochem. and Electrochem. Eng., Vol, , Chap. 3, p. 49. Edited by P. Delahay and C.W. Tobias. Interscience (1962).

16. Galushko, V.P., and Zavgorodynaya, E.F. Ukrain. Khim. Zhur. 11, 2208 (1953).

17. Ivanov, K., and Kudra, O. Zhur. Fiz. Khim. 6, 469 (1935).

18. Kudryavtsev, N.T., Yu Bek, R., and Kushevich, I.F. Zhur. Priklad. Khim. 30, 1093 (1957).

19. Menzies, I.A., Hill, D.L., Hills, G.J., Young, L., and Bockris, J.O'M. J. Electroanalyt. Chem. 1, 161 (1959/60).

20. Inman, D., Hills, G.J., Young, L., and Bockris, J.O'M. Trans. Faraday Soc. 55, 1904 (1959).

21. Kudra, O., and Gitman, E. Zhur. Priklad. Khim. 20, 605 (1947); 21, 284 (1948).

22. Călusaru, A. Electrochim. Acta 12, 1507 (1967).

23. Atanasiu, I., and Călusaru, A. Studii si cercetari de Metalurgie 2, 337 (1957).

24. Leesona Moos Corp. NASA Quart. Repts. Nos. 1 and 2 (1965) NAS-5-9591-Zinc electrode Improvement.

25. Higgins, T.W. Ph.D. Dissertation. Brooklyn Polytechnic (1962).

26. Straumanis, M.E., Reed, J.L., and James, W.J. J. Electrochem. Soc. 14, 885 (1967).

27. Kushner, J.B. J. Electrochem. Soc. 112, 413 (1965).

28. Evans, U.R., and Shome, S.J. Electrodep. Tech. Soc. 27, 45 (1950/51).

29. Powers, R.W. Electrochem. Technol. 5, 429 (1967).

30. Krebs, W.M., and Roe, D.K. J. Electrochem. Soc. 114, 892 (1967).

31. Wranglen, G. Electrochim. Acta 2, 130 (1960).

32. Yang, L., Chein, C., and Hudson, R.G. J. Electrochem. Soc. 106, 632 (1959).

33. Faust, F.W., and John, H.F. J. Electrochem. Soc. 108, 109 (1961).

34. Giron, I., and Ogburn, F.J. Electrochem. Soc. 108, 842 (1961).

35. Ogburn, F., Paretzkin, B., and Peisar, H.S. Acta Cryst. 17, 774 (1964).

36. Ogburn, F., Bechtoldt, C., Morris, J.B., and De Koranyi, A. J. Electrochem. Soc. 112, 574 (1965).

37. Hamilton, D.R., and Seidensticker, R.G. J. Appl. Phys. 31, 1165 (1960).

38. Faust, F.W., and John, H.F. J. Electrochem. Soc. 110, 463 (1963).

39. Cohen, J.B., and Weertman, J. Acta Met. 11, 996 (1963).

40. Stachurski, Z. Investigation and Improvement of Zinc Electrodes for Electrochemical Cells, Final Rept. (1965). Yardney Electric Corp., New York.

41. Farr, J.P.G., and Hampson, N.A. J. Electroanalyt. Chem. 13, 433 (1967).

42. McBreen, J. Study to Investigate and Improve the Zinc Electrode for Spacecraft Electrochemical Cells. Second Quart. Rept. June 1967. Yardney Electric Company, New York.

LEGENDS FOR FIGURES

Fig. 1 Electrolytic Cell — Plan and Side view.

2 Typical dendritic growth resulting from a low propagation rate experiment. $C_0 = 0.01$ moles liter^{-1}, $T = 35°C$, $\eta = -100$ mv., $g = 2.4\,\mu\text{min}^{-1}$.

3 Typical dendritic growth resulting from a high propagation rate experiment. $C_0 = 0.1$ moles liter^{-1}, $T = 35°C$, $\eta = -100$ mv., $g = 24.0\,\mu\,\text{min}^{-1}$.

4 Example of the zinc deposition obtained at $\eta = -200$ mv; $C_0 = 0.1$ moles liter^{-1}, $T = 35°C$.

5 Total current against time as a function of zincate concentration C_0 (moles liter^{-1}). $\eta = -100$ mv. and $T = 35°C$.

6 Initial predendrite current density as a function of zincate concentration C_0 when $\eta = -100$ mv. and $T = 35°C$.

7 Total current against time as a function of overpotential when $C_0 = 0.1$ moles liter^{-1} and $T = 35°C$.

8 Total current against time as a function of electrolyte temperature T, when $C_0 = 0.1$ moles liter^{-1} and $\eta = -100$ mv.

9 Dendrite length against time as a function of zincate concentration C_0 (moles liter^{-1}), when $\eta = -100$ mv and $T = 35°C$.

10 Log dendrite tip current density i as a function of zincate concentration C_0, when $\eta = -100$ mv and $T = 35°C$. The broken line represents the slope of 0.75 as given by eqn. (52).

Fig. 11 Dendrite length against time as a function of overpotential, when C_0 = 0.1 moles liter^{-1} and T = 35°C.

12a Dendrite propagation rate (g) as a function of overpotential. C_0 = 0.1 moles liter^{-1} and T = 35°C.

12b Dendrite tip current density (i) as a function of overpotential. C_0 = 0.1 moles liter^{-1} and T = 35°C.

13 Dendrite length against time as a function of electrolyte temperature T. C_0 = 0.1 moles liter^{-1} and η = -100 mv.

14 Arrhenius-type plot expressing the relationship between the dendrite tip current density (i) and the reciprocal temperature, when C_0 = 0.1 moles liter^{-1} and η = -100 mv.

15 Model of diffusion controlled deposition onto microrough surface.

16 Idealized representation of dendrite initiation, due to a microrough surface, at equal intervals of relative time $\frac{t}{\tau}$, where τ is defined as in eqn. (20).

17 Total current against time as a function of the initial roughness of the pre-formed zinc cathode. Experimental conditions: C_0 = 0.1 moles liter^{-1}, η = -92 mv, and T = 35°C. A is the smooth initial surface formed at a low c.d., whereas B is the rough initial surface formed at a high c.d.

18 Log $(i - i_{L, O})$ against time as a function of zincate concentration C_0, where η = -100 mv. and T = 35°C as per eqn. (26).

Fig. 19 $\text{Log}(i - i_{L,O})$ against time as a function of overpotential, when $C_0 = 0.1$ moles liter^{-1} and $T = 35°C$.

20 $\text{Log}(i - i_{L,O})$ against time as a function of electrolyte temperature T, when $C_0 = 0.1$ moles liter^{-1} and $\eta = -100$ mv.

21 Plot of $(\tau C_0)^{1/2}$ against $(C_0)^{1/4}$ as per eqn. (28); τ values obtained from the slopes of Figure 18 and assuming $\beta = 0.5$.

22 Arrhenius plot for $\log \tau$ against the reciprocal temperature as per eqn. (32) or (33).

23 Arrhenius plot for log initial pre-dendrite current density against the reciprocal temperature.

24 Plot of $(\tau)^{\frac{1}{2}}$ against $\exp(\frac{\beta F}{RT} \cdot \eta)$ for eqn. (37) under the assumption of $i_0 = 100$ mAcm^{-2} (solid line) and $i_0 = 23$ mAcm^{-2} (broken line). $C_0 = 0.1$ moles liter^{-1} and $T = 35°C$.

25 Normalized dendrite tip current density (i) against the normalized dendrite tip radii (r_n) for zinc deposition under the following conditions: $C_0 = 0.1$ moles liter^{-1}, $T = 35°C$, $i = 12$ mAcm^{-2}, $\gamma = 2000$ ergs cm^{-2}, and $\delta_0 = 10^{-3}$ cm.

26 i_n against r_n for the deposition of silver from ionic melts (Barton and Bockris[1]) taking $C_{ag} = 0.5$ moles liter^{-1}, $i_0 = 50$ Acm^{-2}, $D = 1.4 \times 10^{-5}$ cm^2 sec^{-1}, $T = 581°K$, $\gamma = 2000$ ergs cm^{-2}, and $\delta_0 = 0.02$ cm.

27 i_n against r_n for zinc deposition from alkaline zincate solutions as a function of the exchange current density i_0. C_0 = = 0.1 moles liter^{-1}, $T = 35°C$, $\eta = -100$ mv, $\gamma = 2000$ ergs cm^{-2}, and $\delta_0 = 10^{-3}$ cm.

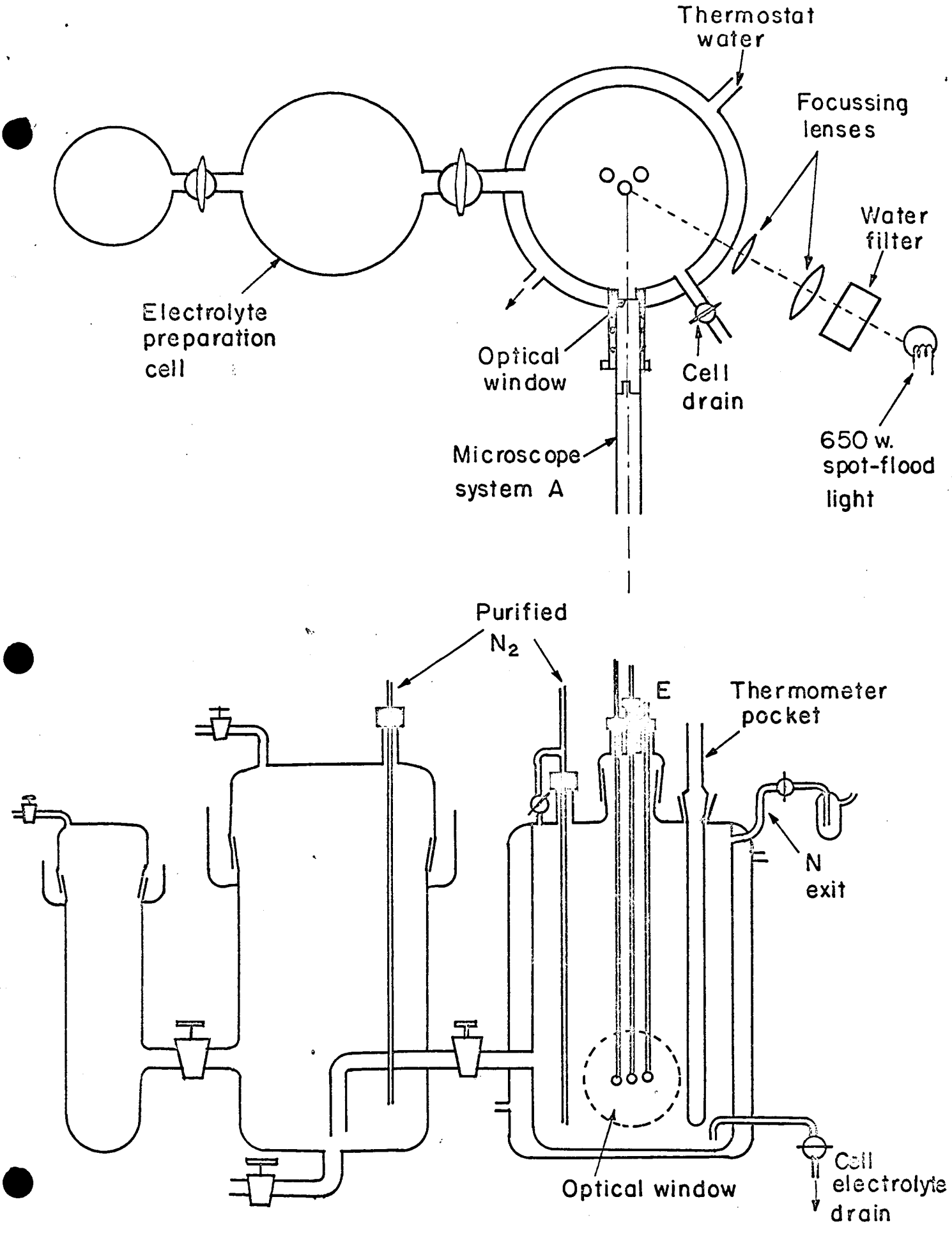

Fig. 1 Electrolyte cell - plan and side elevation.

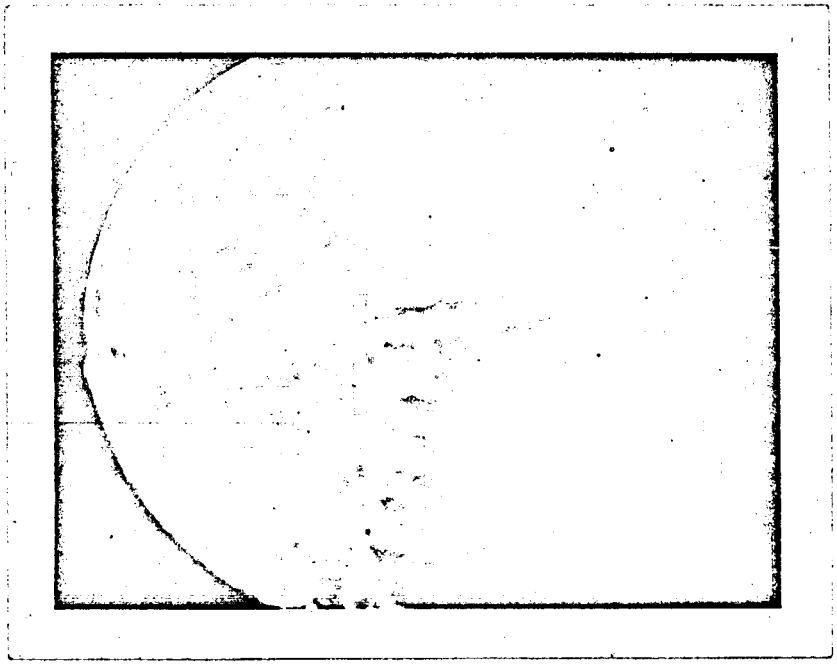

Fig. 2

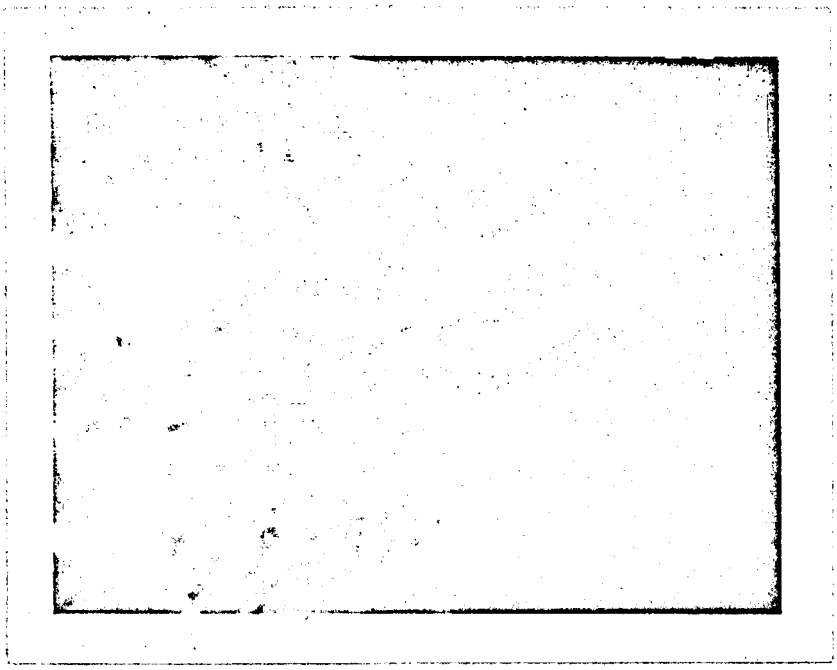

Fig. 3

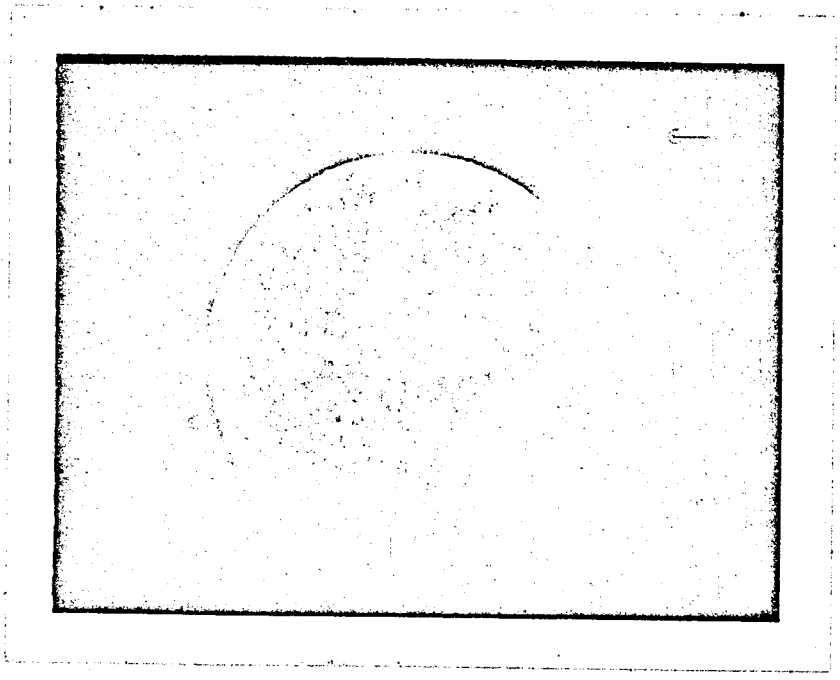

Fig. 4

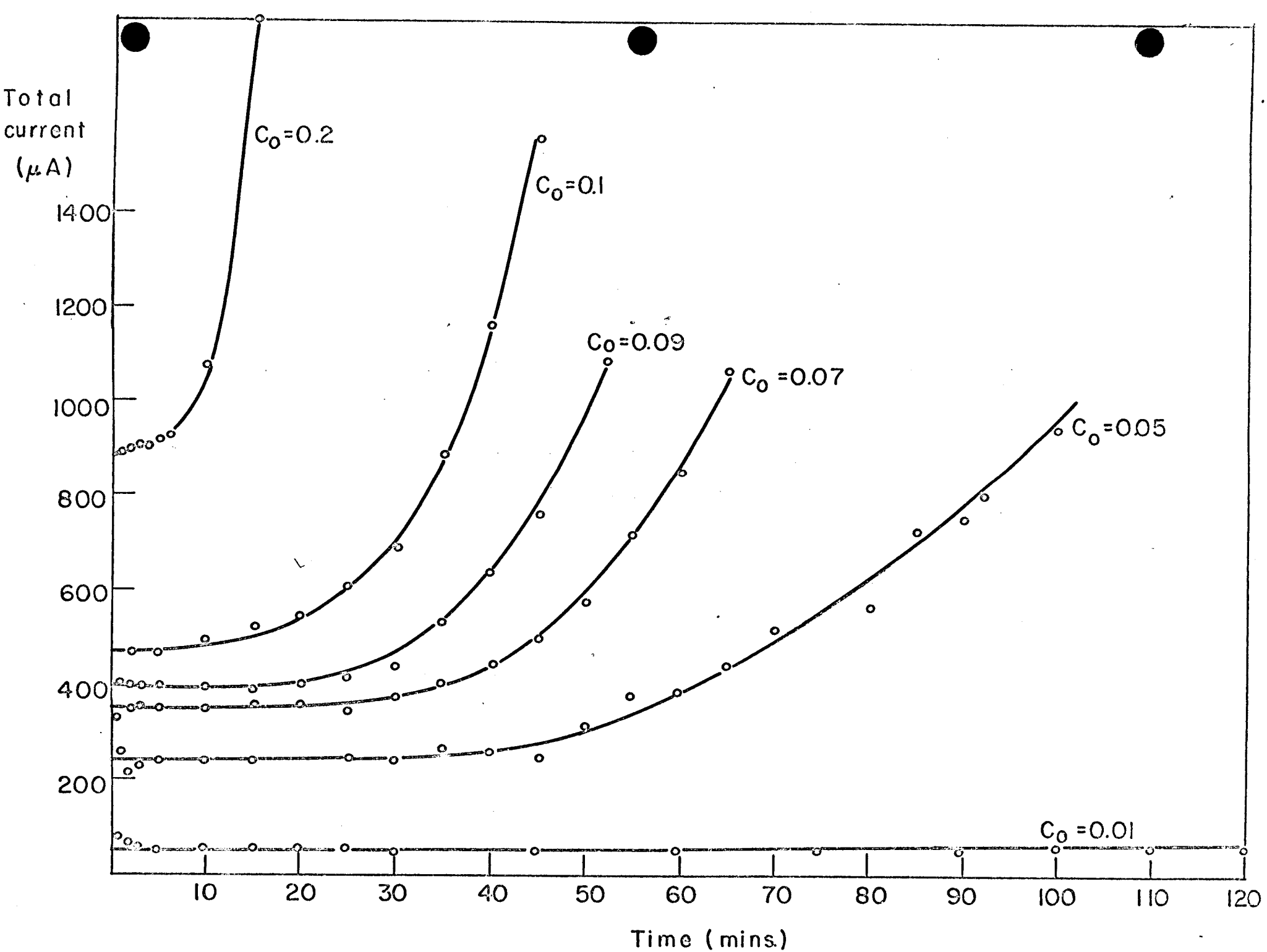
Total current (μA)
1400
1200
1000
800
600
400
200
C_0=0.2
C_0=0.1
C_0=0.09
C_0 =0.07
C_0=0.05
C_0 =0.01
10
20
30
40
50
60
70
80
90
100
110
120
Time (mins.)

Fig. 5

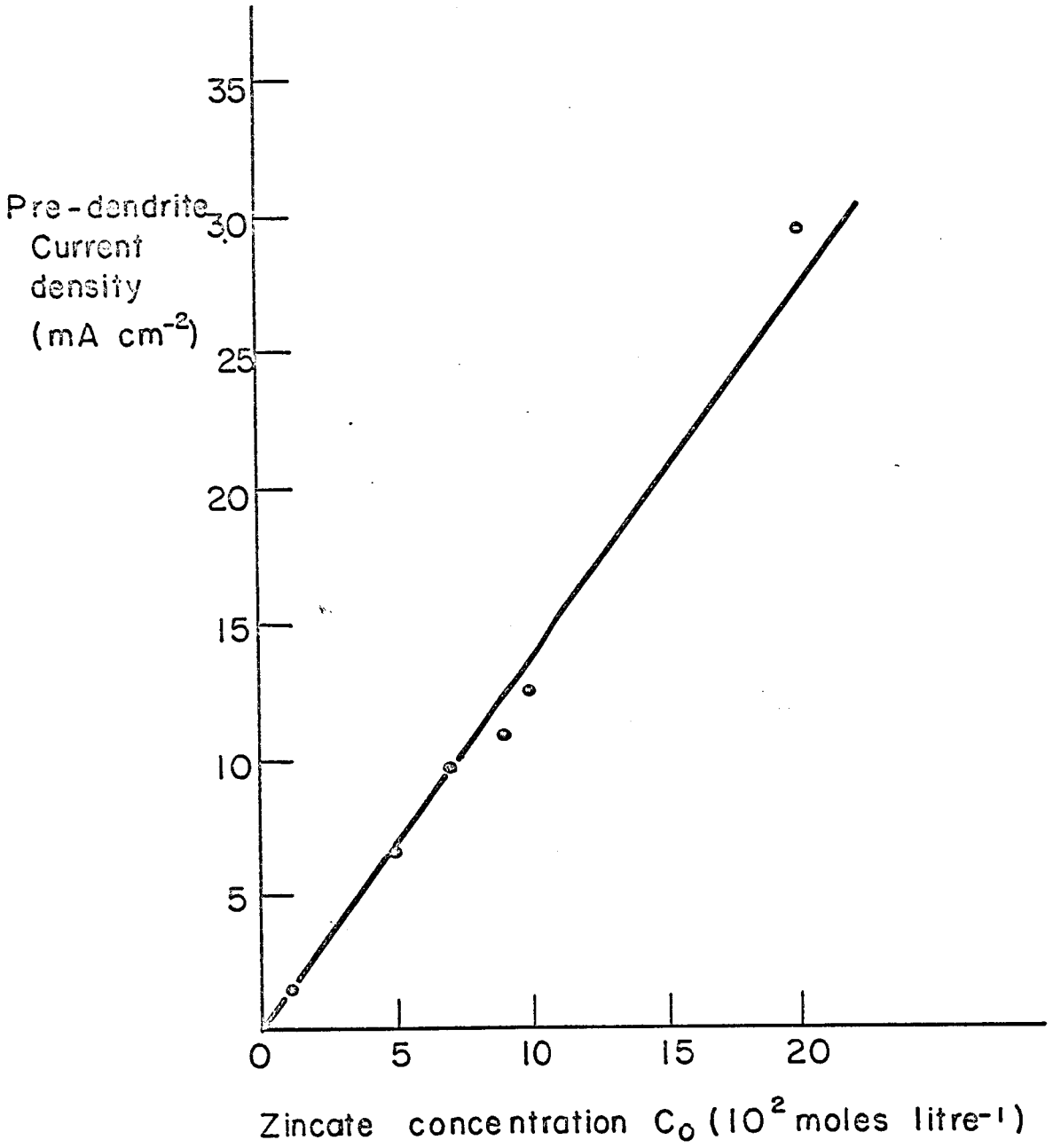
Pre-dendrite Current density (mA cm^{-2})
35
30
25
20
15
10
5
0
5
10
15
20
Zincate concentration C_0 (10^2 moles litre^{-1})

Fig. 6

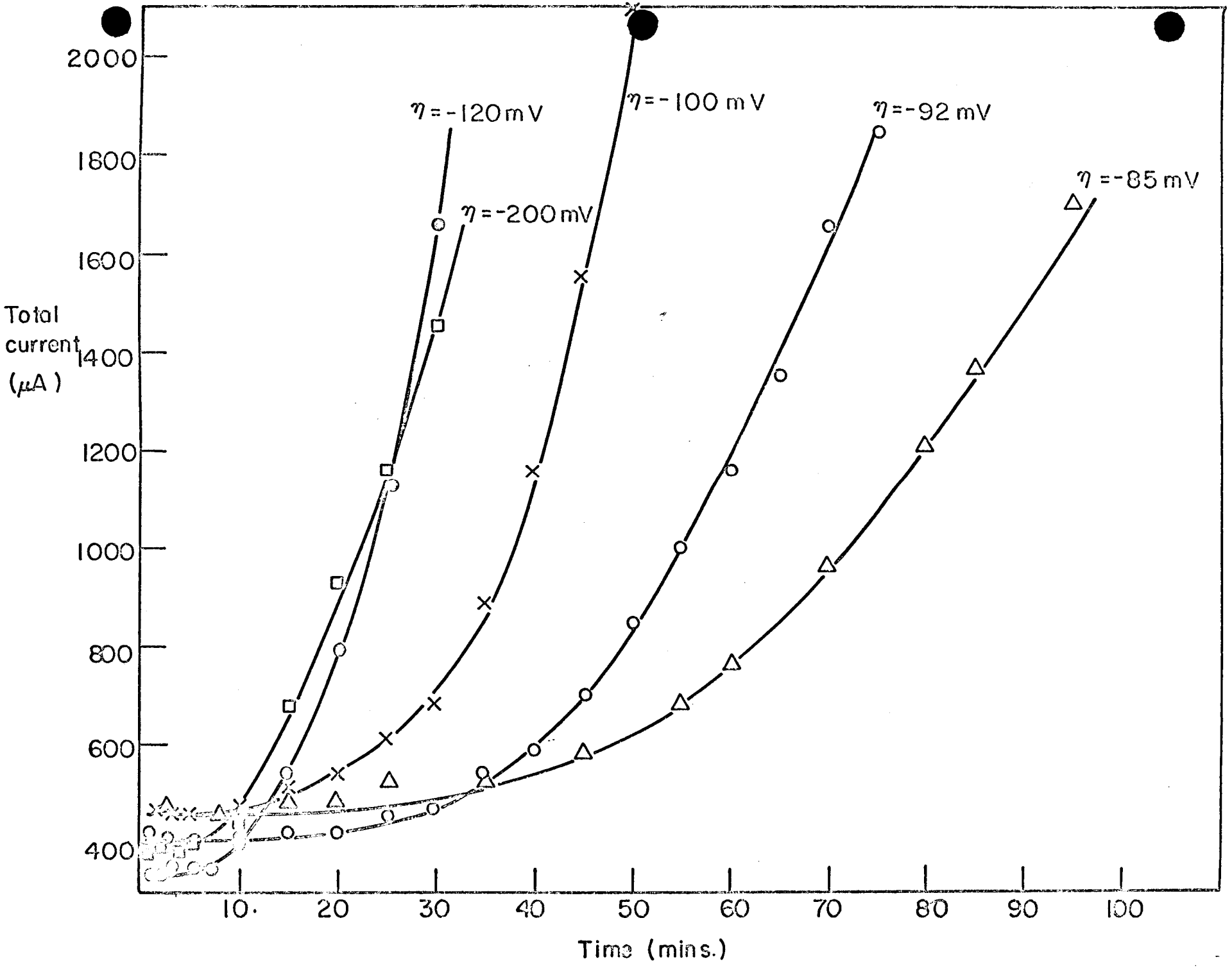
η = -120 mV
η = -100 mV
η = -92 mV
η = -85 mV
η = -200 mV
Total current (μA)
2000
1800
1600
1400
1200
1000
800
600
400
10
20
30
40
50
60
70
80
90
100
Time (mins.)

Fig.7

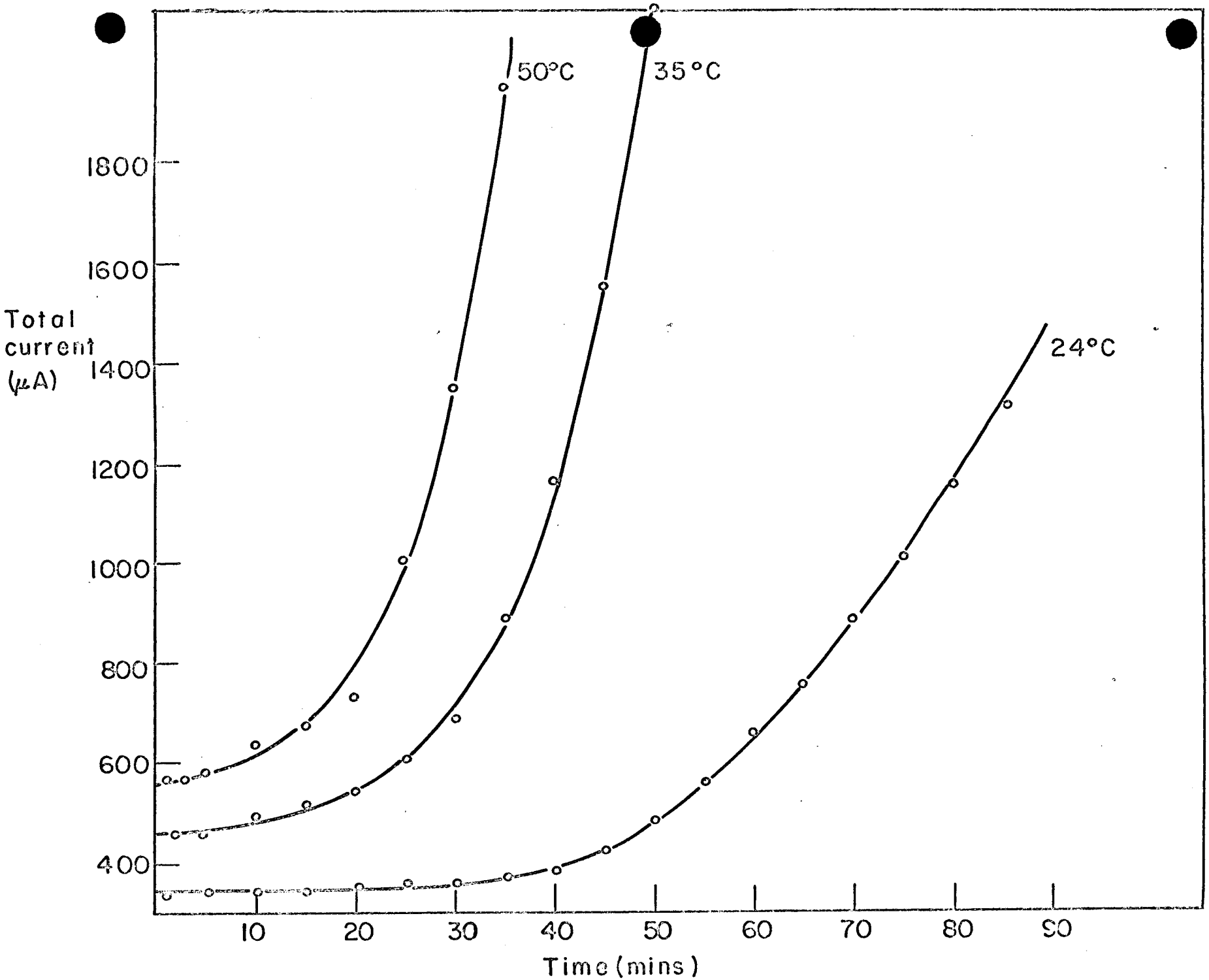
50°C
35°C
24°C
1800
1600
1400
1200
1000
800
600
400
Total current (μA)
10
20
30
40
50
60
70
80
90
Time (mins)

Fig. 8

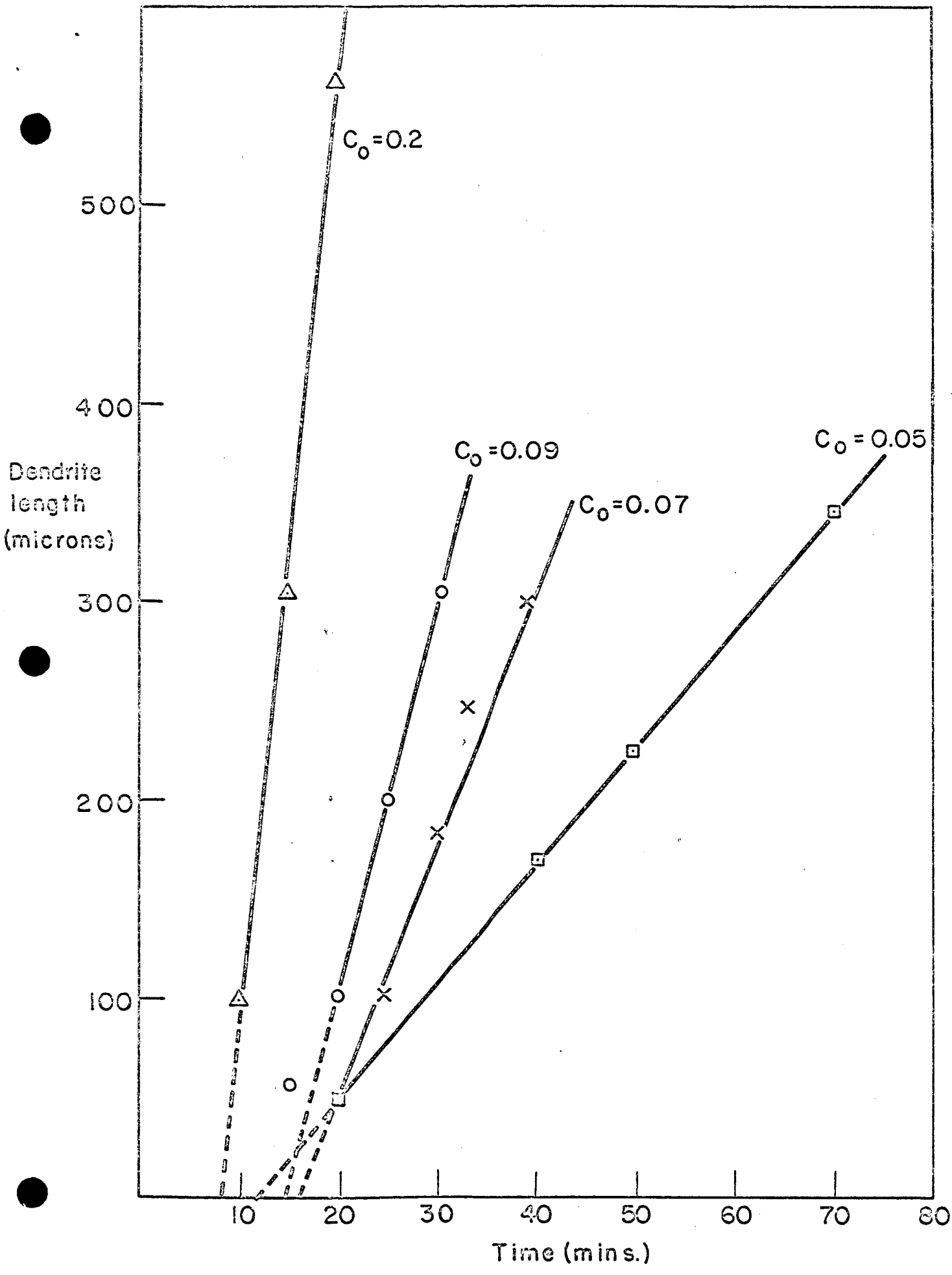
C_0=0.2
C_0=0.09
C_0=0.07
C_0=0.05
500
400
300
200
100
Dendrite length (microns)
10
20
30
40
50
60
70
80
Time (mins.)

Fig. 9

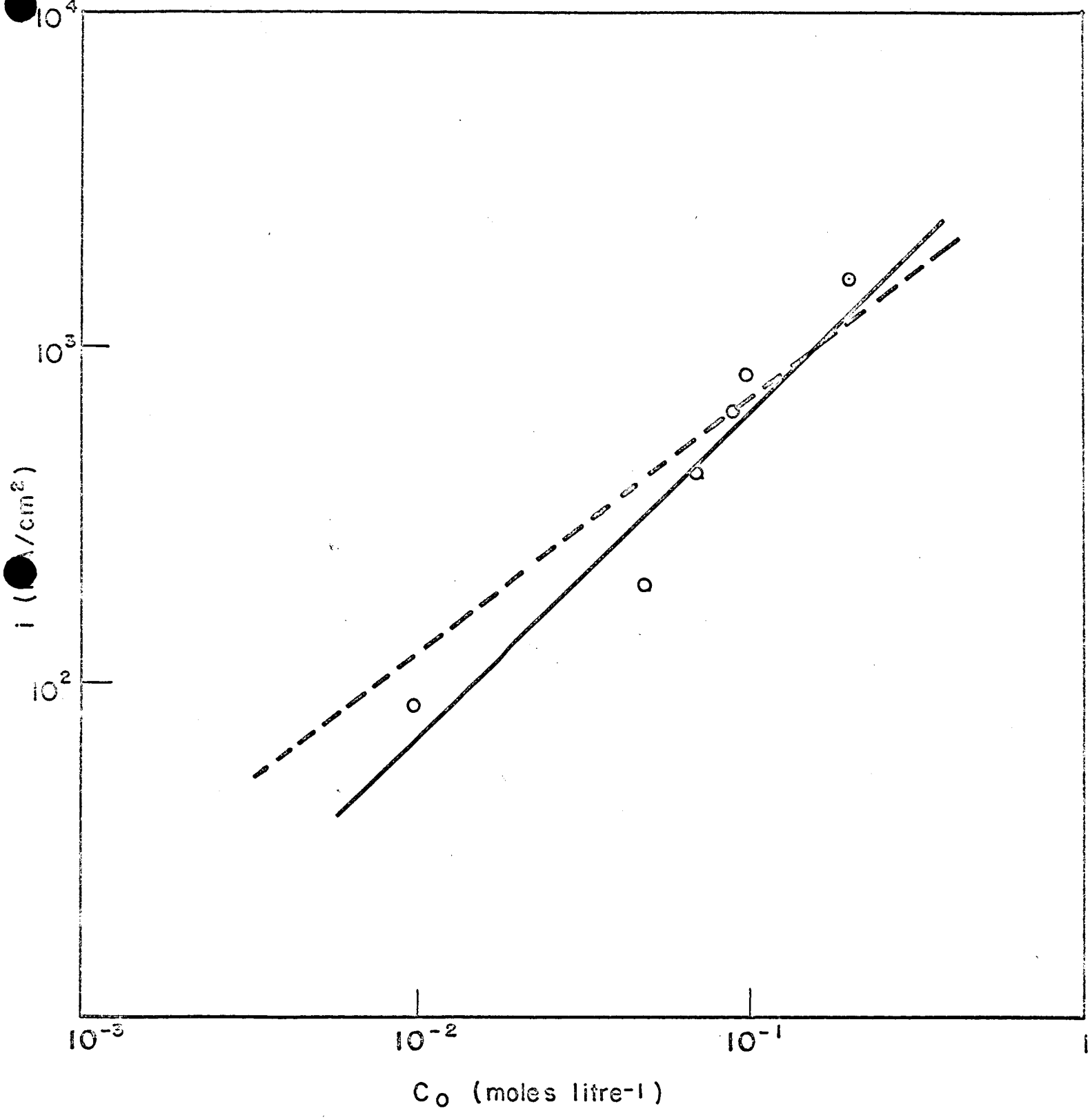

Fig. 10

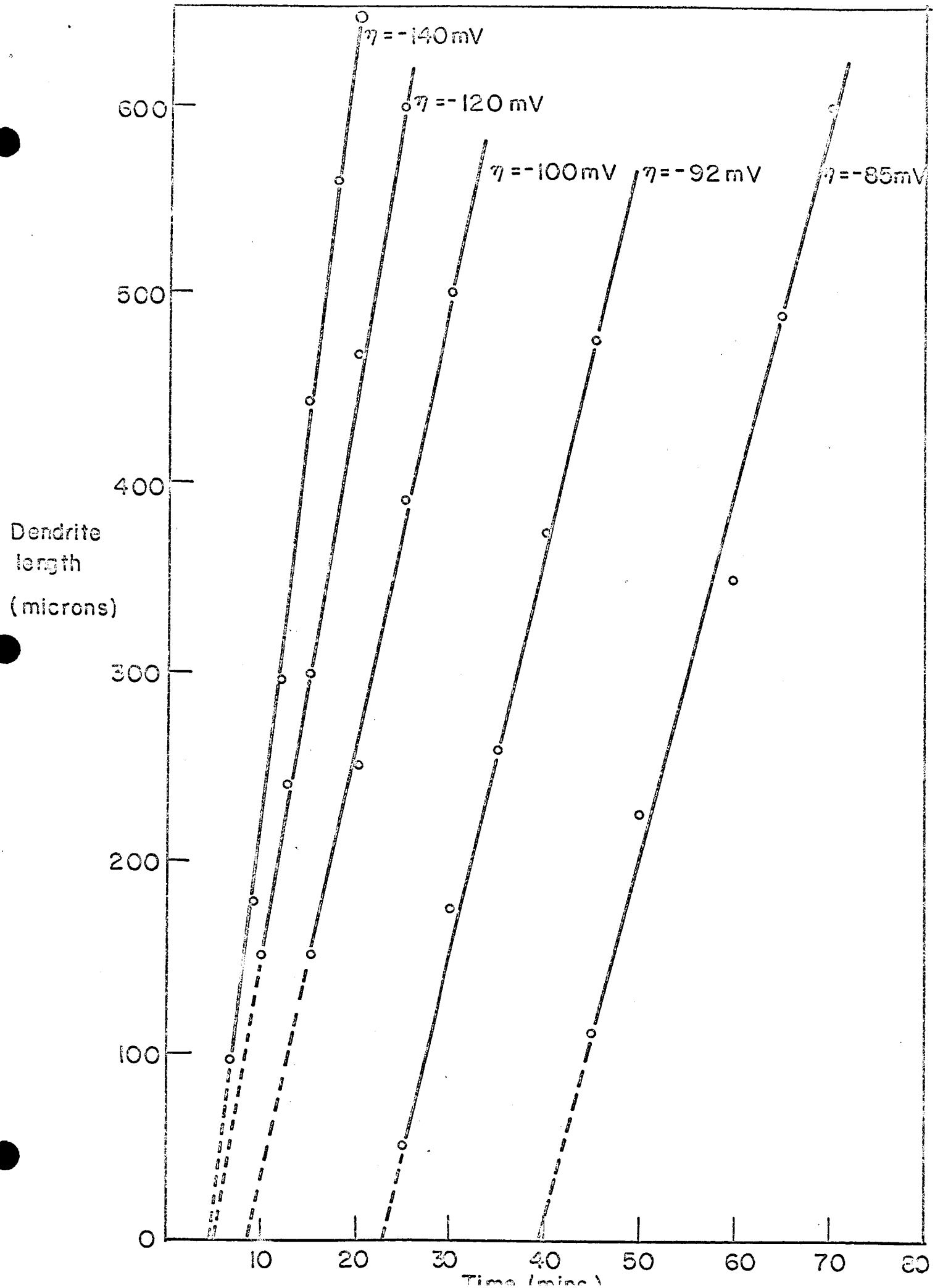
η = -140 mV
η = -120 mV
η = -100 mV
η = -92 mV
η = -85 mV
600
500
400
300
200
100
0
Dendrite length (microns)
10
20
30
40
50
60
70
80
Time (mins)

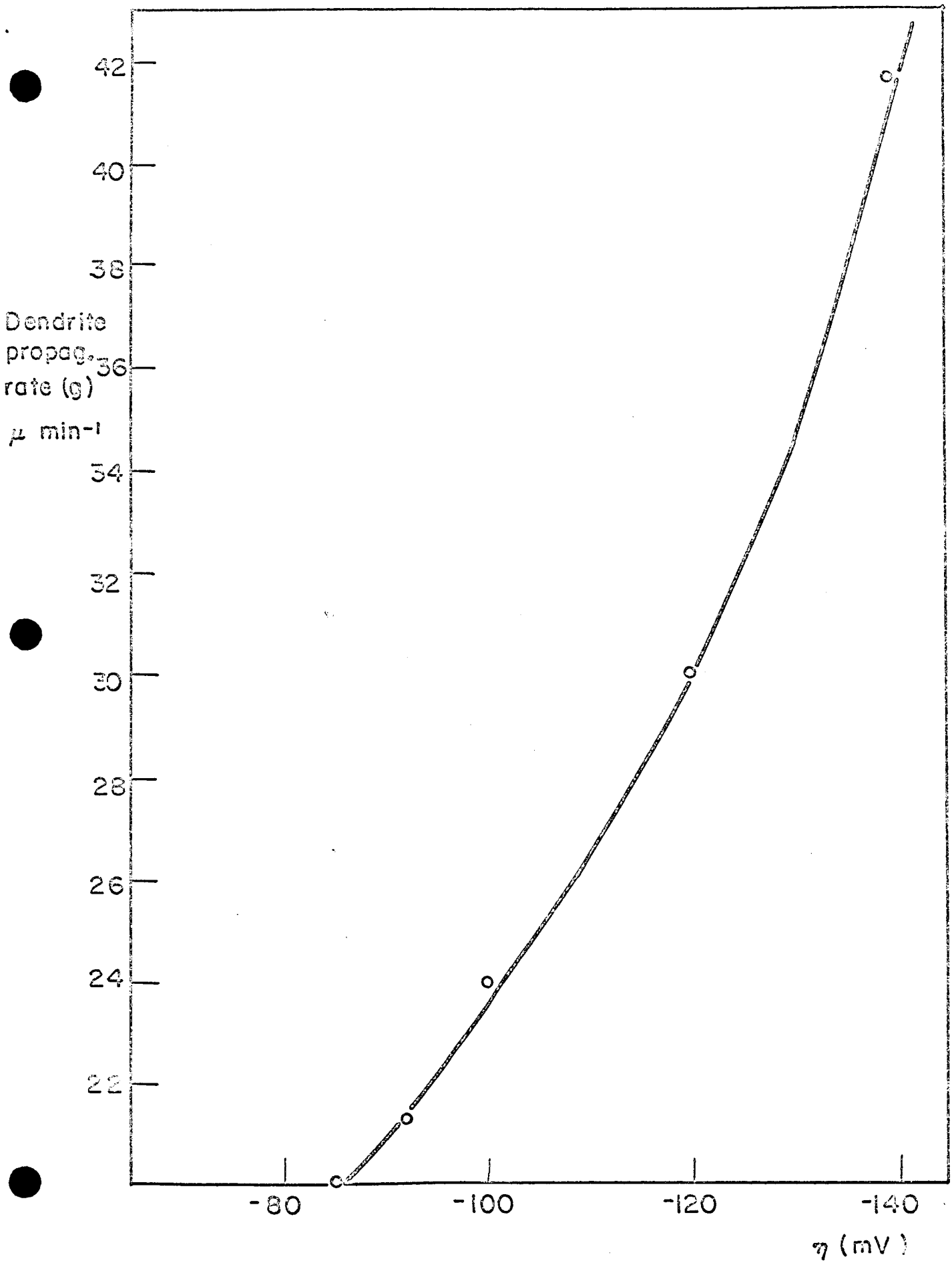
42
40
38
Dendrite propag. rate (g) μ min-1
36
34
32
30
28
26
24
22
-80
-100
-120
-140
η (mV)

Fig.12a

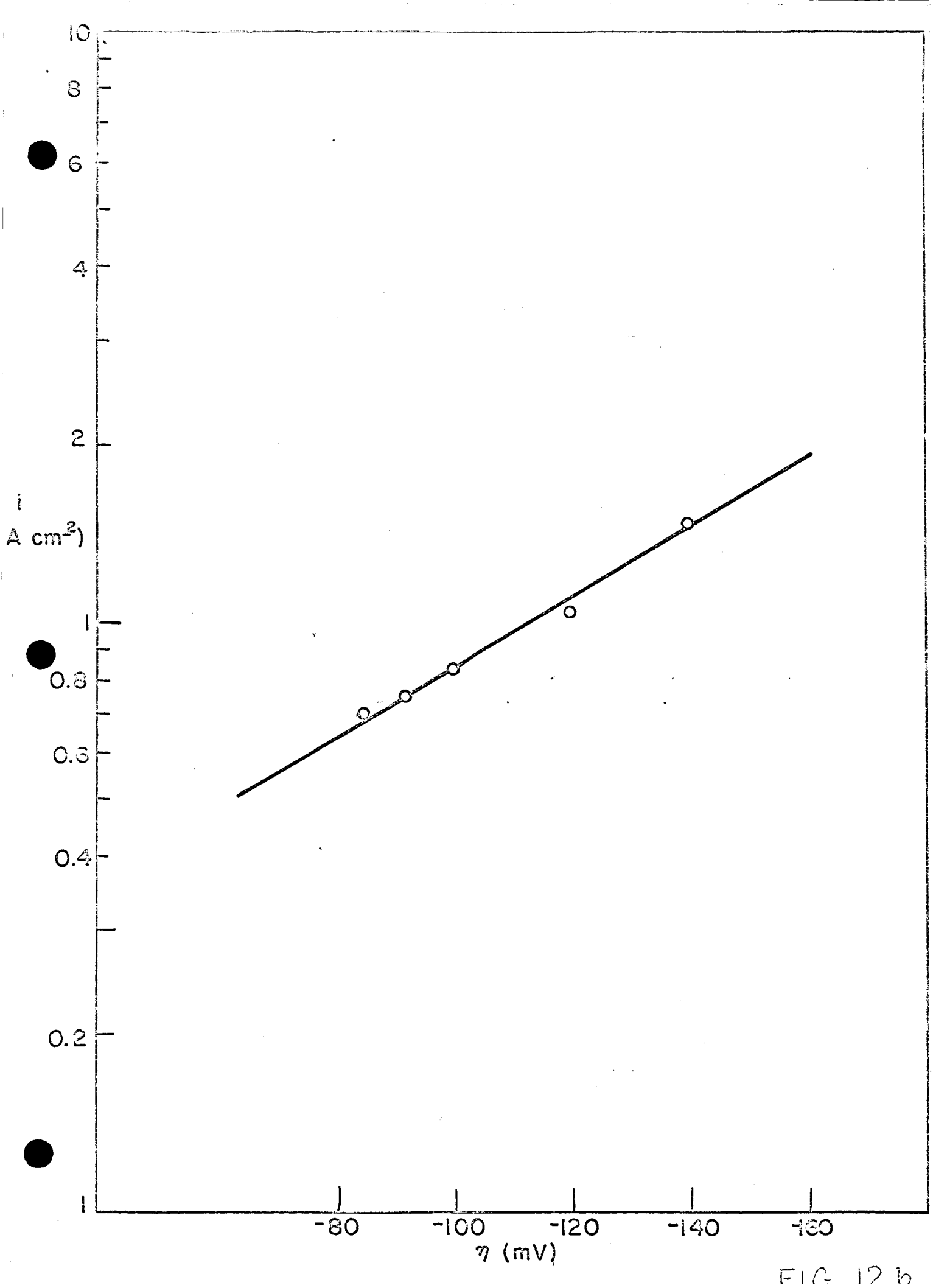

FIG. 12 b

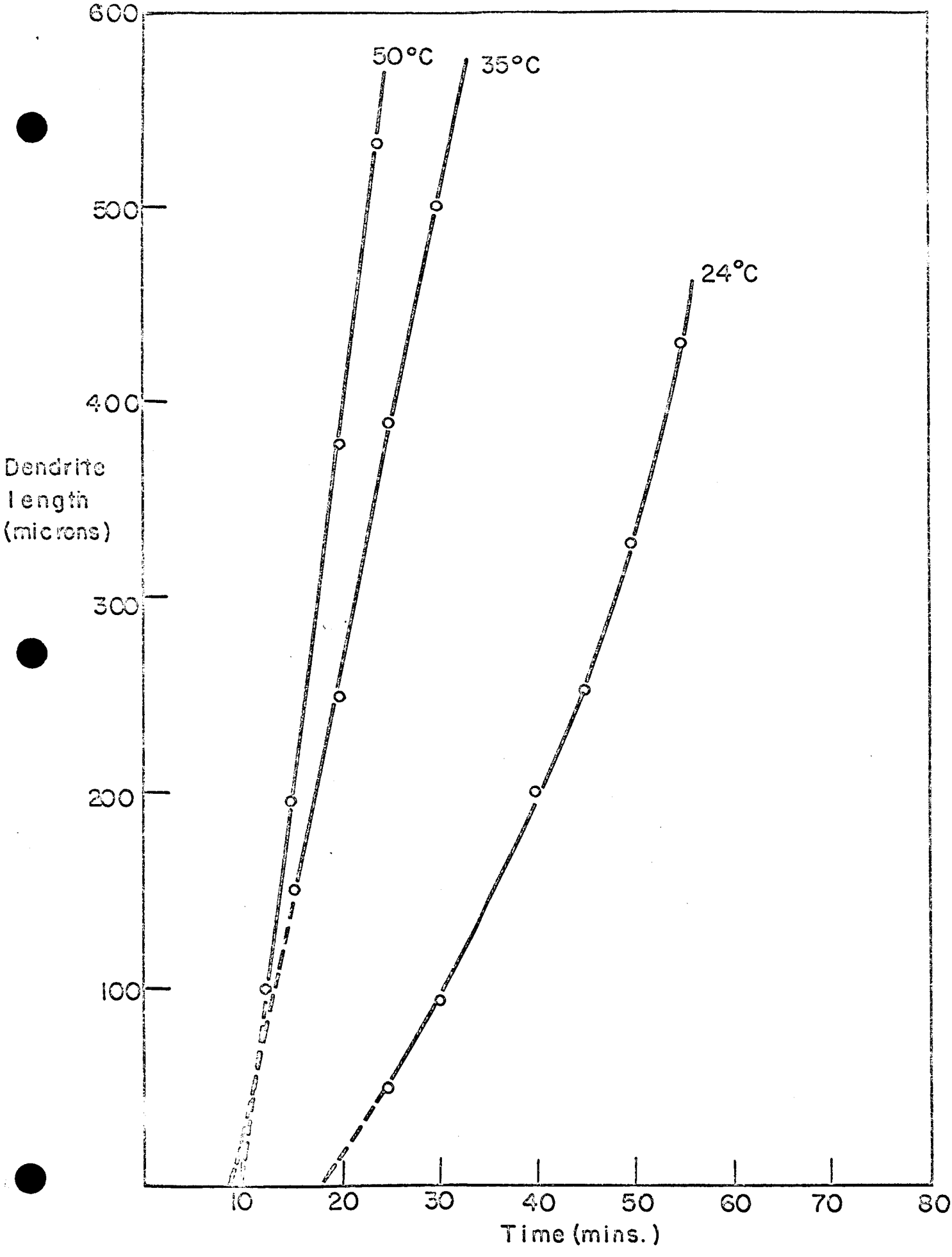
600
500
400
300
200
100
Dendrite length (microns)
50°C
35°C
24°C
10
20
30
40
50
60
70
80
Time (mins.)

Fig. 13

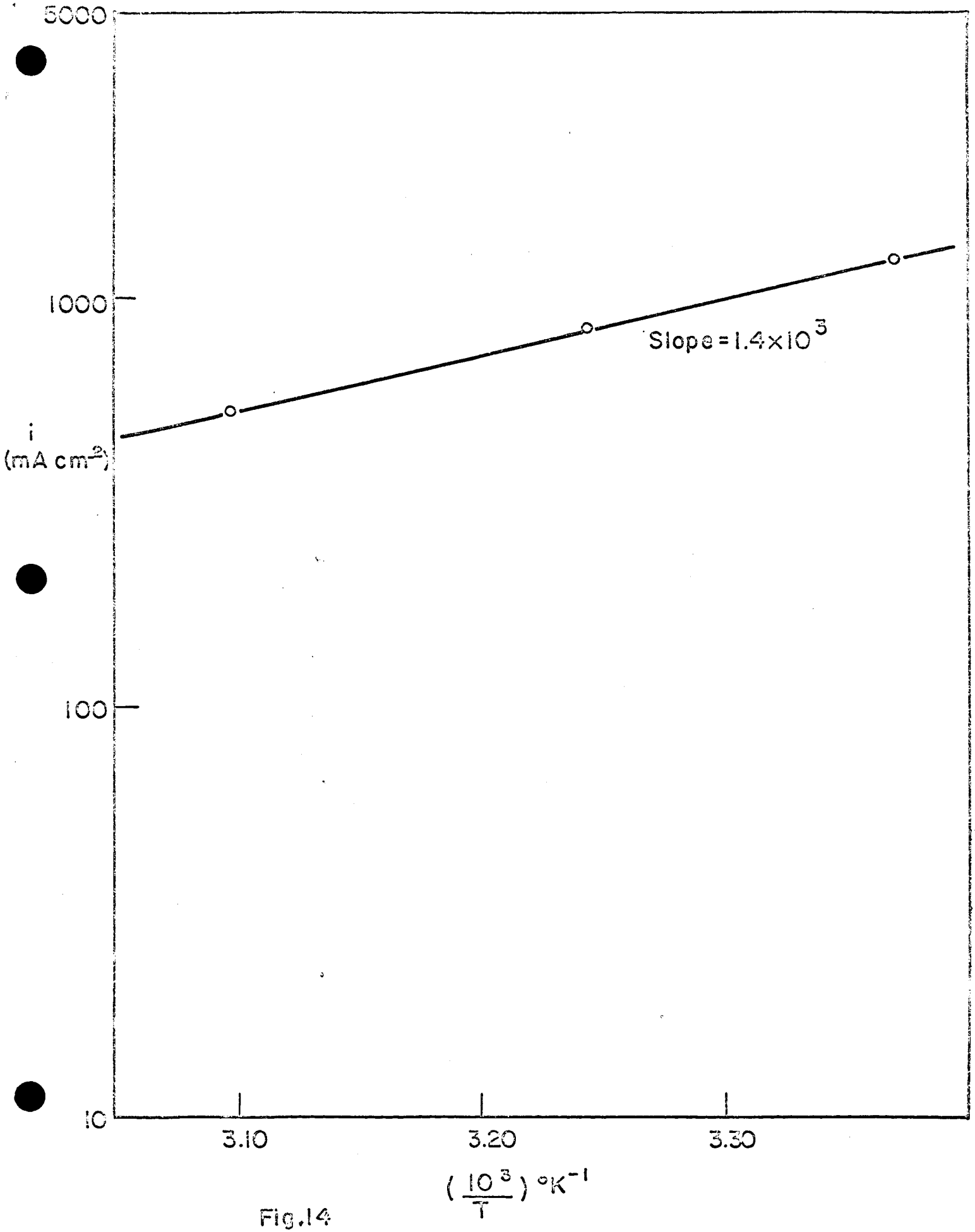
5000
1000
100
10
i
(mA cm^{-2})
Slope = 1.4×10^{3}
3.10
3.20
3.30
$\left(\frac{10^3}{T}\right)$ °K^{-1}

Fig.14

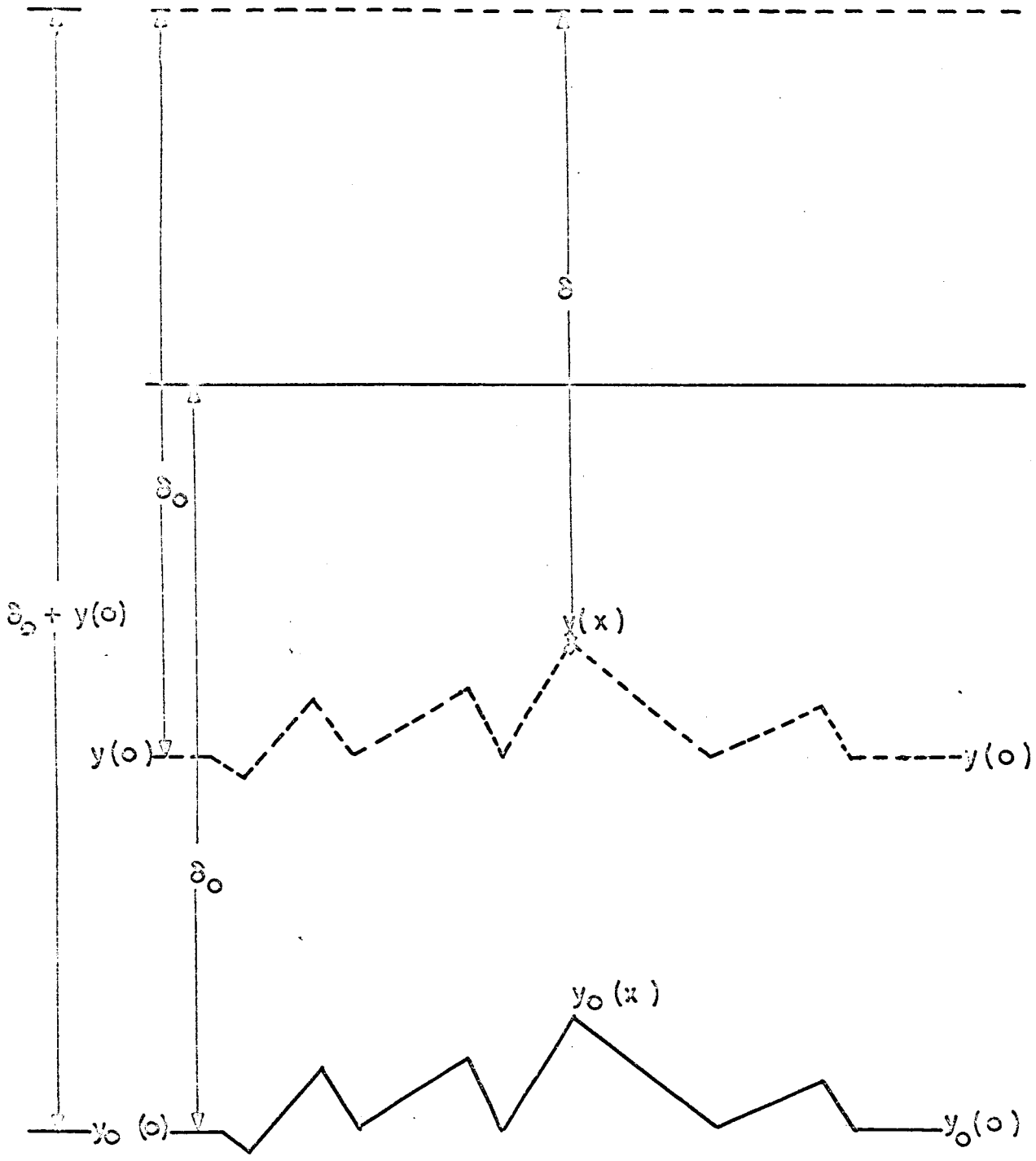

Fig. 15

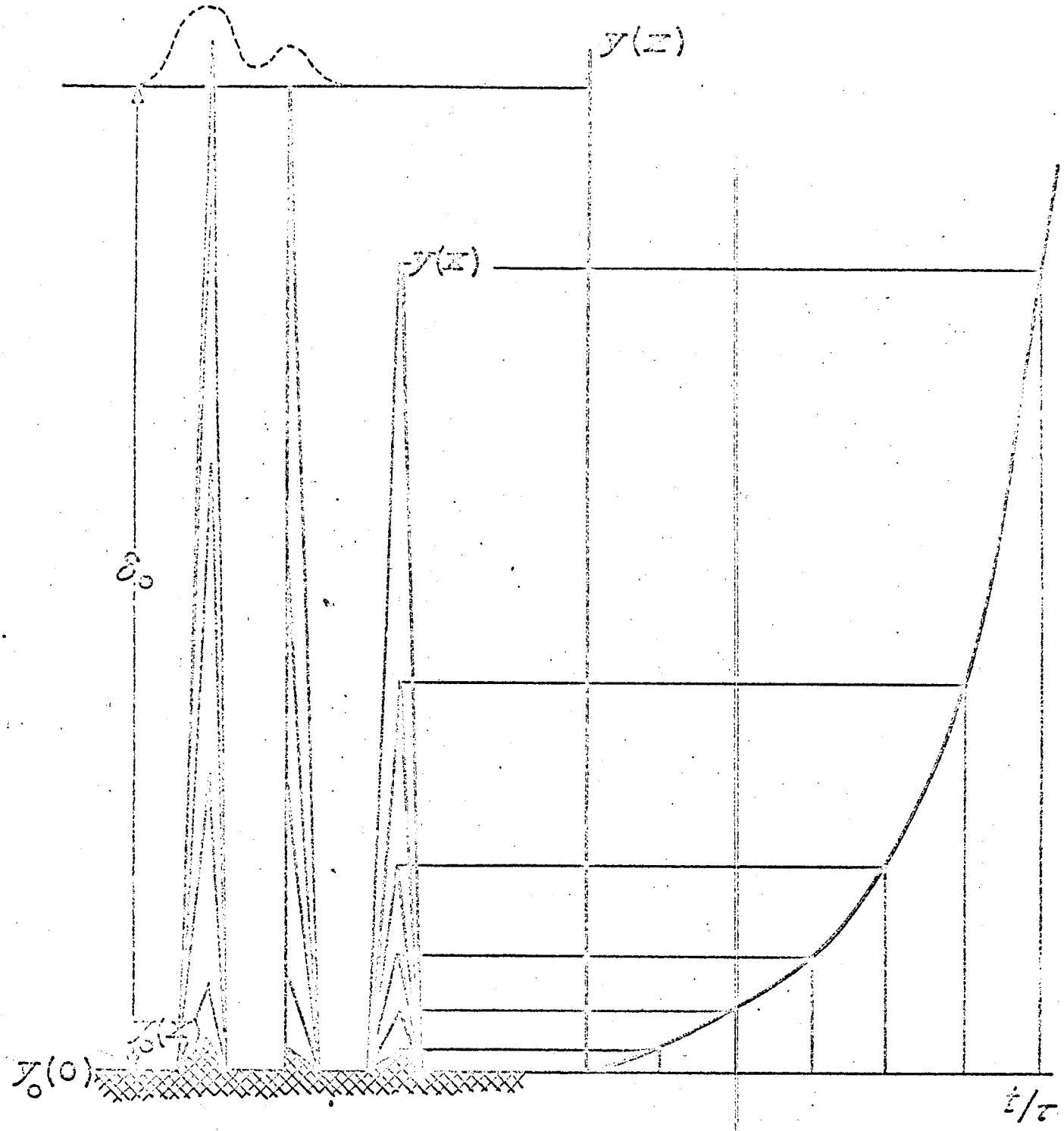

FIG. 16

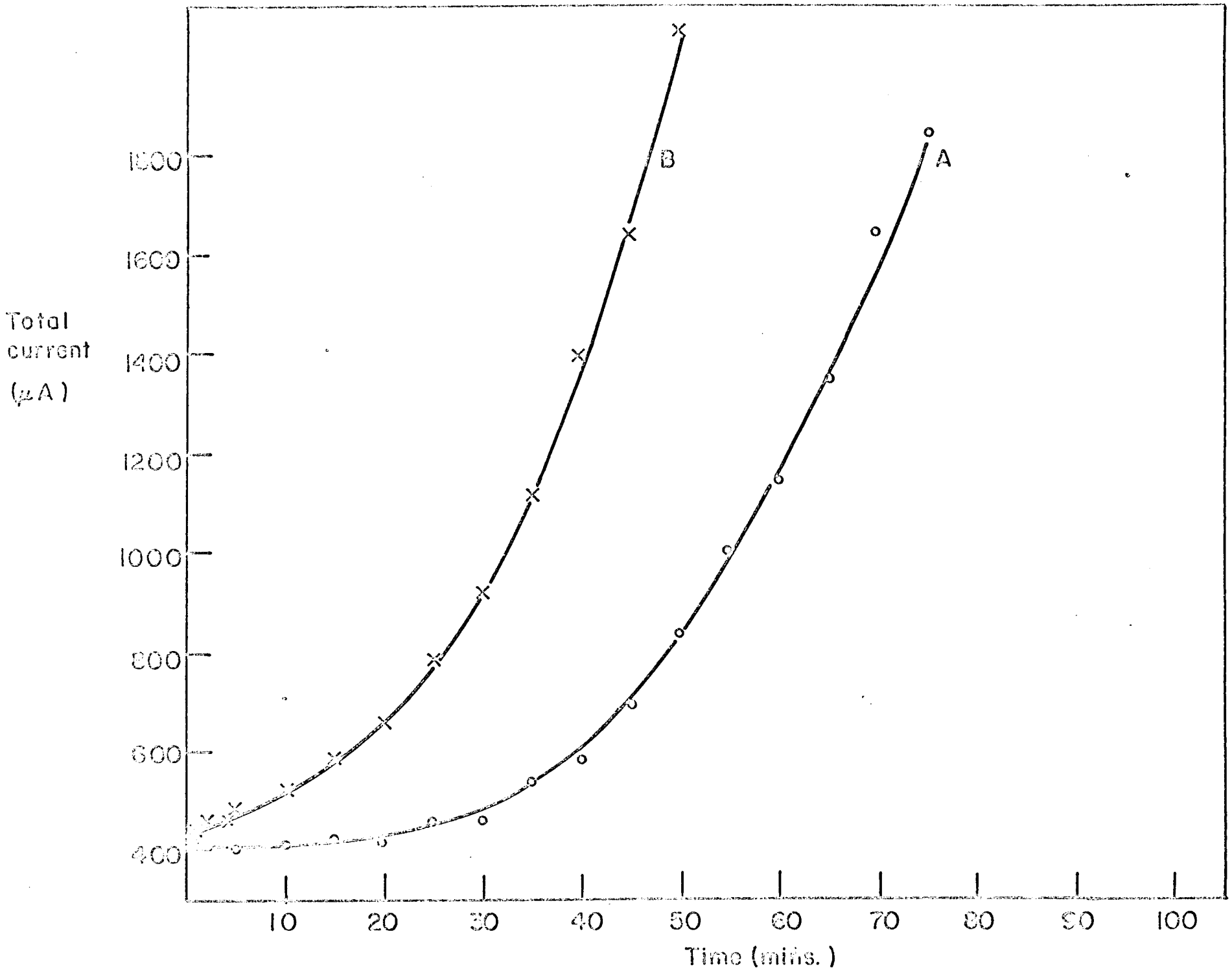
Total current (μA)
1800
1600
1400
1200
1000
800
600
400
B
A
10
20
30
40
50
60
70
80
90
100
Time (mins.)

Fig. 17

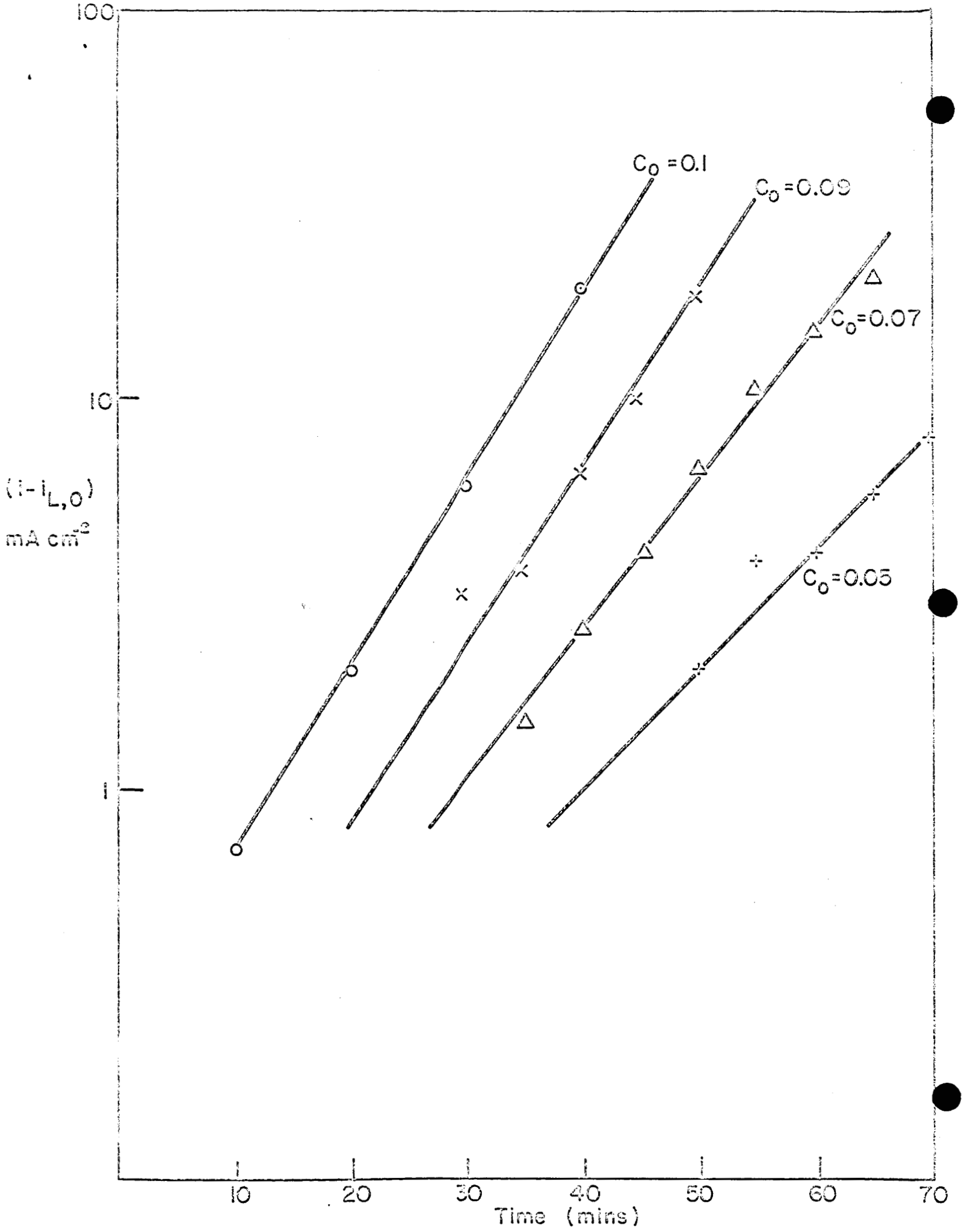
100
10
1
$(i-i_{L,o})$
mA cm^{-2}
C_o = 0.1
C_o = 0.09
C_o = 0.07
C_o = 0.05
10
20
30
40
50
60
70
Time (mins)

Fig. 18

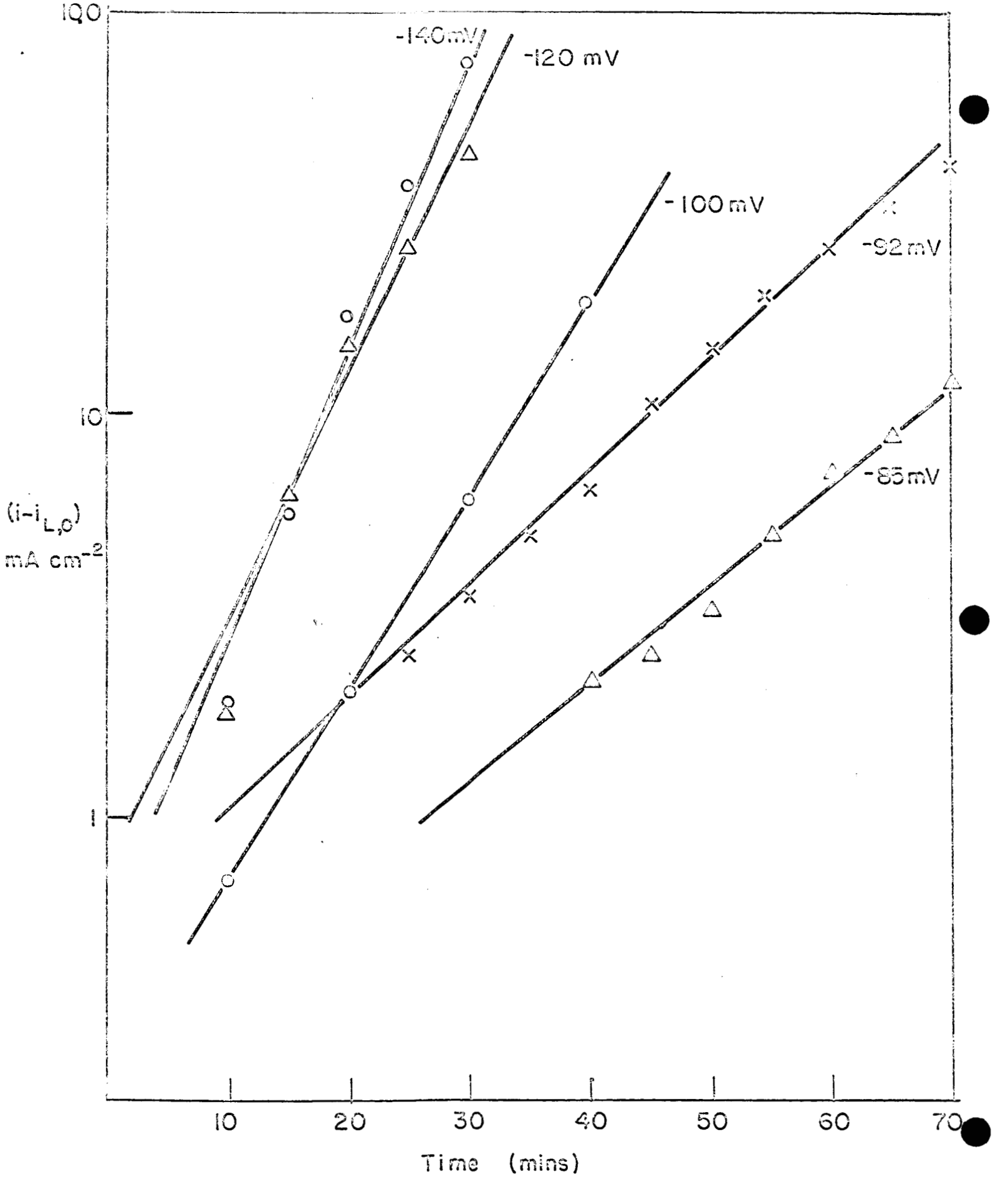
100
10
1
$(i-i_{L,c})$
mA cm^{-2}
-140mV
-120 mV
-100mV
-92mV
-85mV
10
20
30
40
50
60
70
Time (mins)

Fig. 19

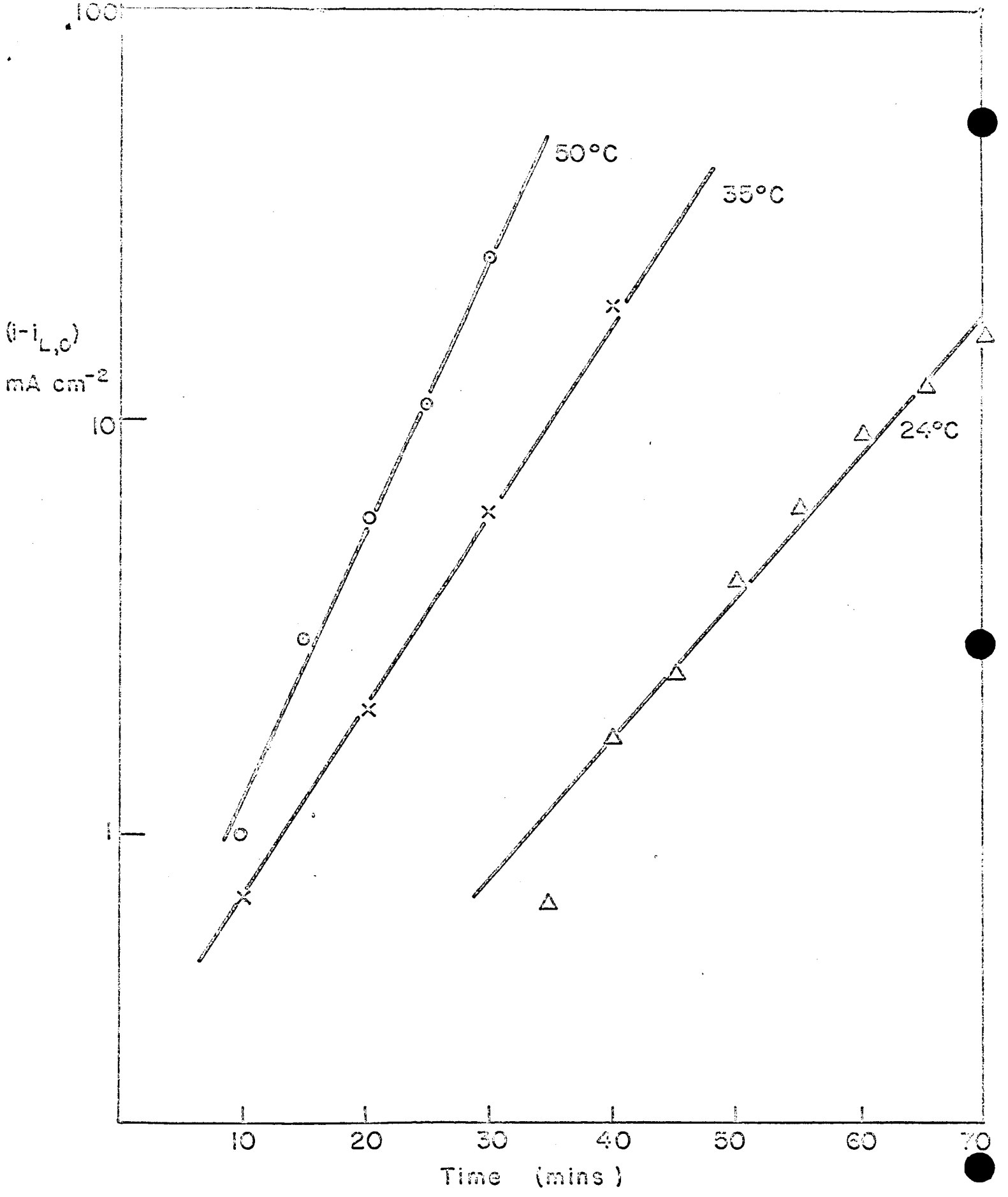

Fig. 20

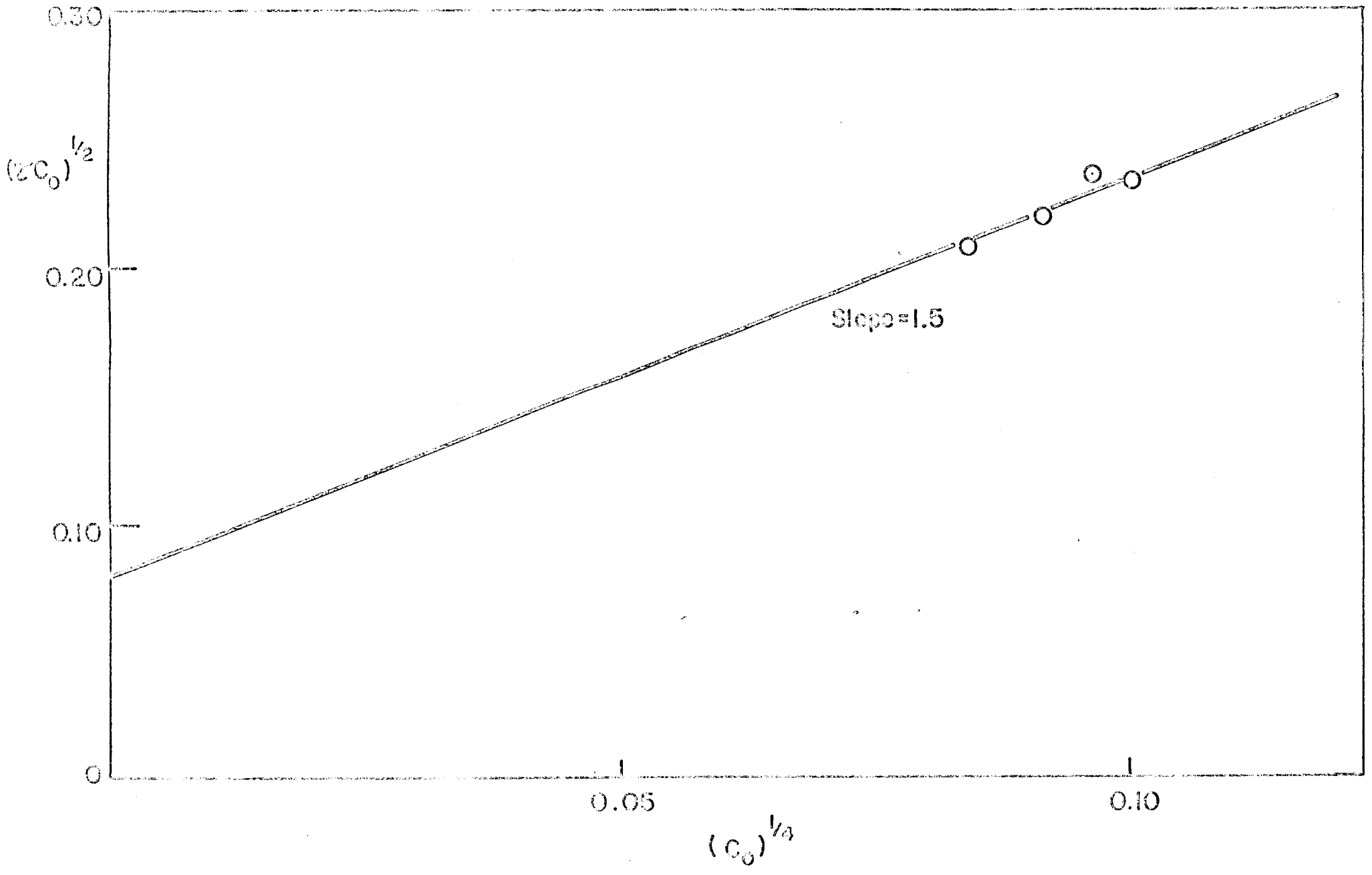

Fig. 2

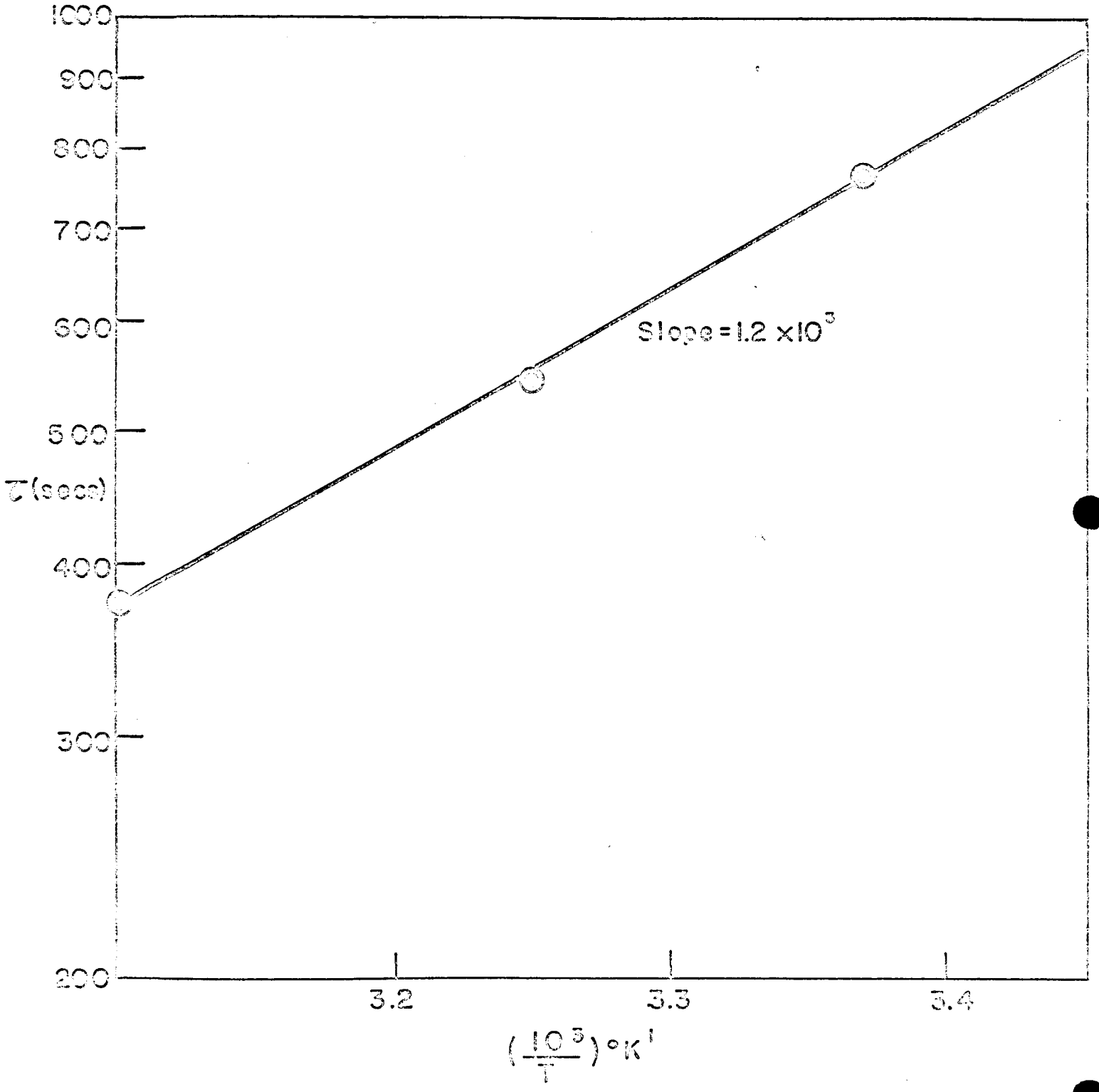
1000
900
800
700
600
500
400
300
200
τ(secs)
Slope = 1.2 x 10³
3.2
3.3
3.4
(10³/T) °K⁻¹

Fig. 22

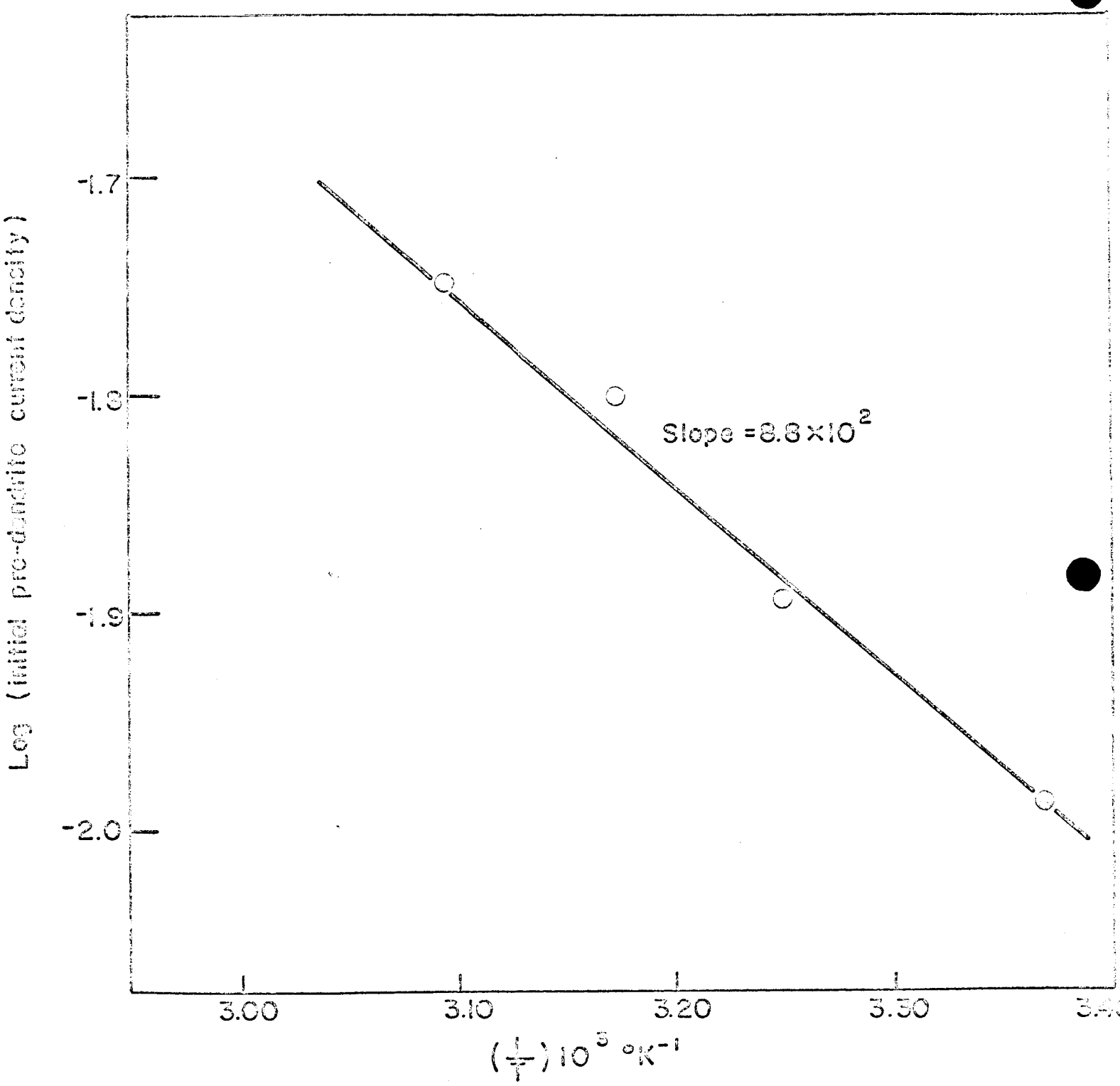
Log (initial pre-dendritic current density)
-1.7
-1.8
-1.9
-2.0
Slope = 8.8 × 10²
3.00
3.10
3.20
3.30
(1/T) 10³ °K⁻¹

Fig. 25

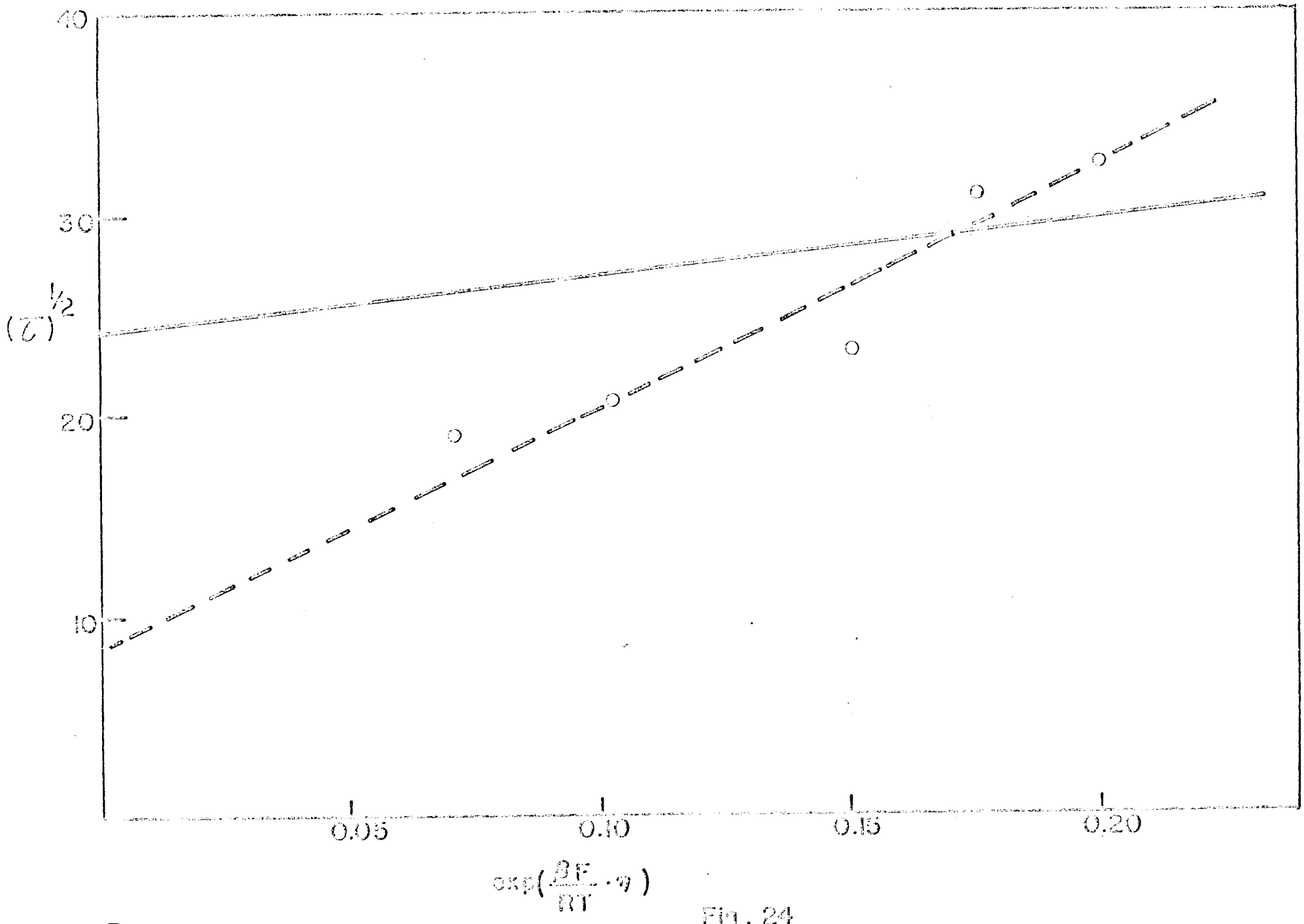
40
30
20
10
$(\mathcal{C})^{1/2}$
0.05
0.10
0.15
0.20
$\exp\left(\frac{\beta F}{RT} \cdot \varphi\right)$

Fig. 24

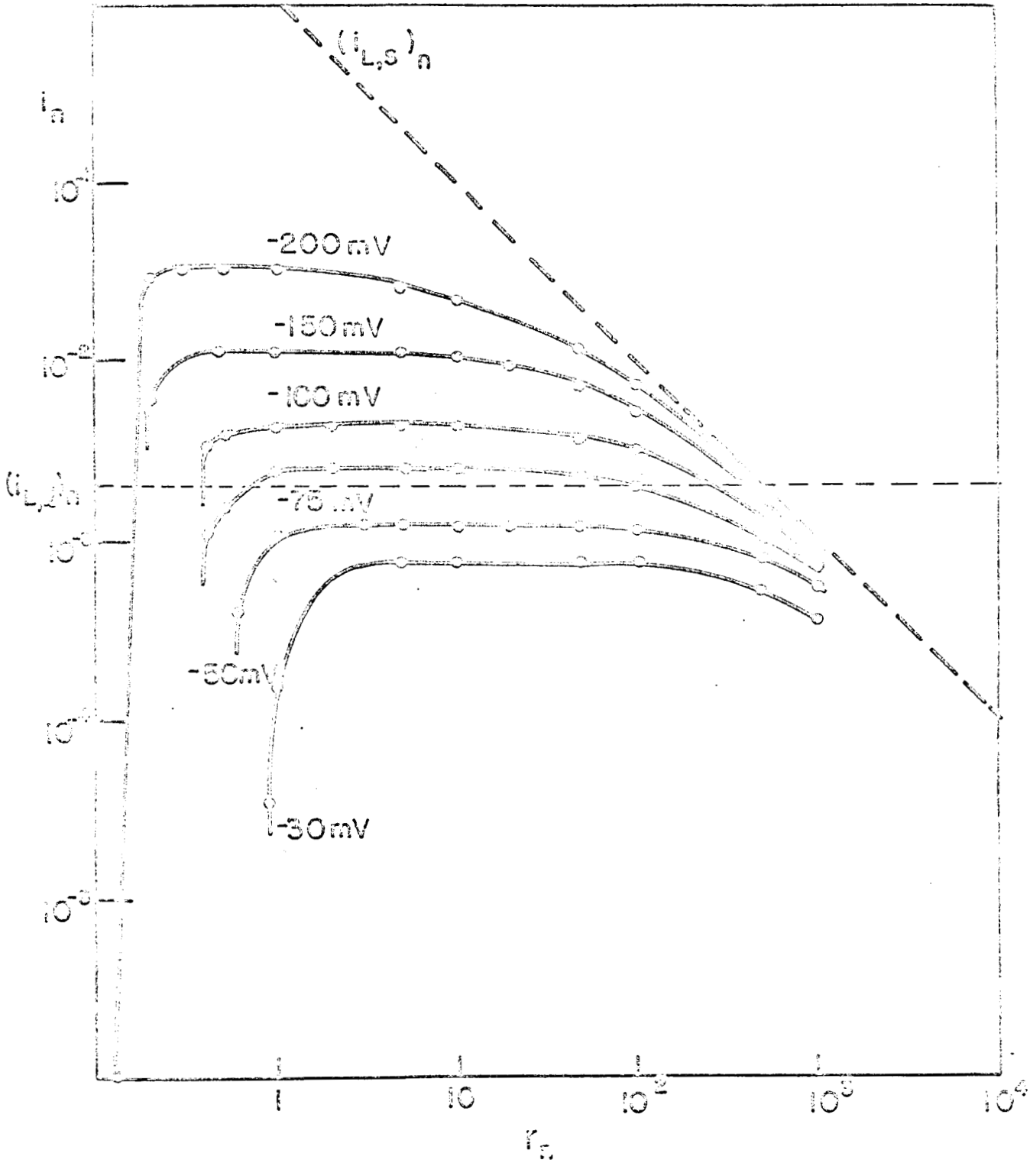
$(i_{L,s})_n$
i_n
10^{-1}
-200 mV
-150 mV
10^{-2}
-100 mV
$(i_{L,d})_n$
-75 mV
10^{-3}
-50mV
10^{-4}
-30 mV
10^{-5}
1
10
10^2
10^3
10^4
r_n

Fig. 25

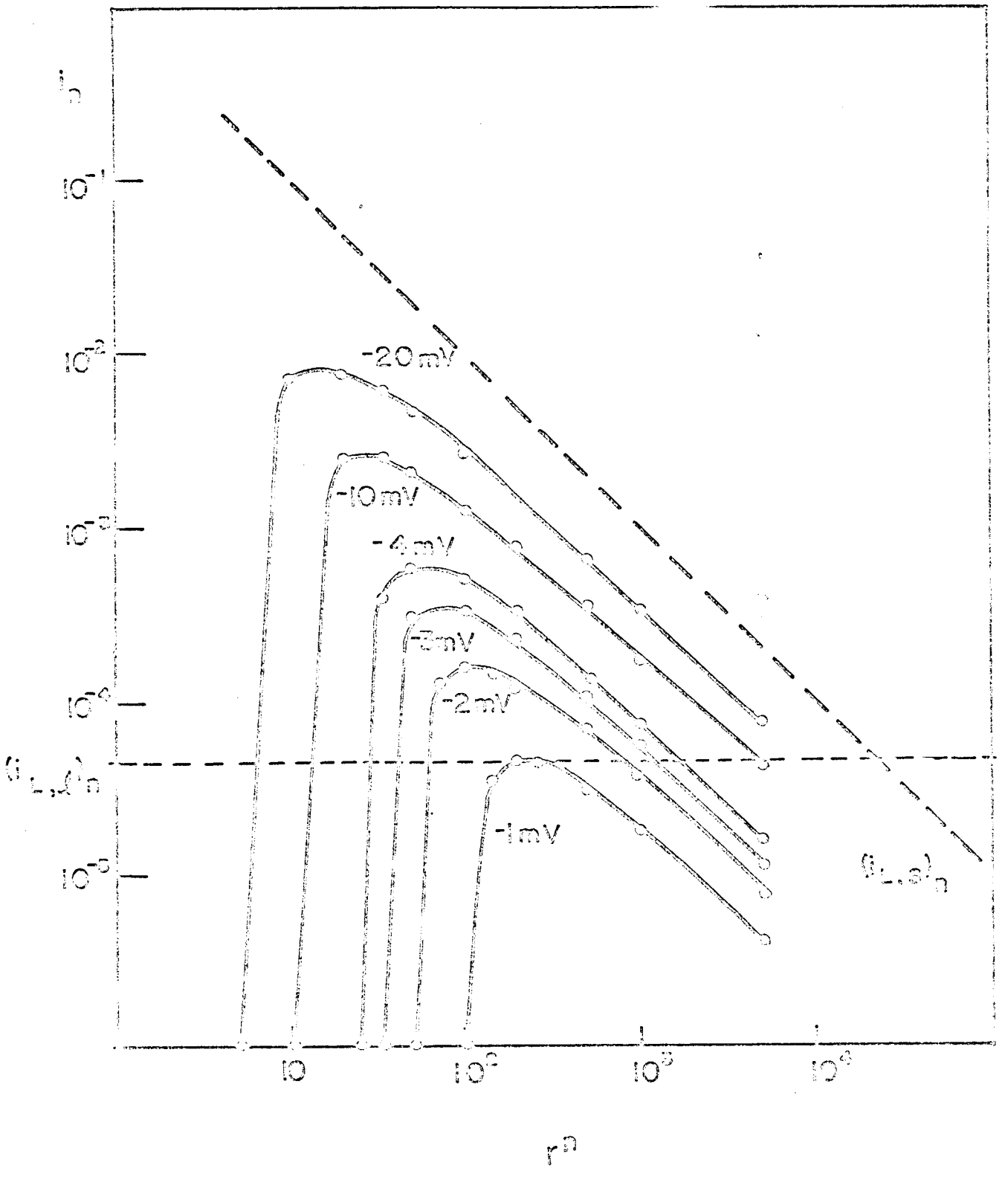
i_n
10^{-1}
10^{-2}
10^{-3}
10^{-4}
10^{-5}
$(i_{L,A})_n$
-20 mV
-10 mV
-4 mV
-3 mV
-2 mV
-1 mV
$(i_{L,S})_n$
10
10^2
10^3
10^4
r^n

Fig. 26

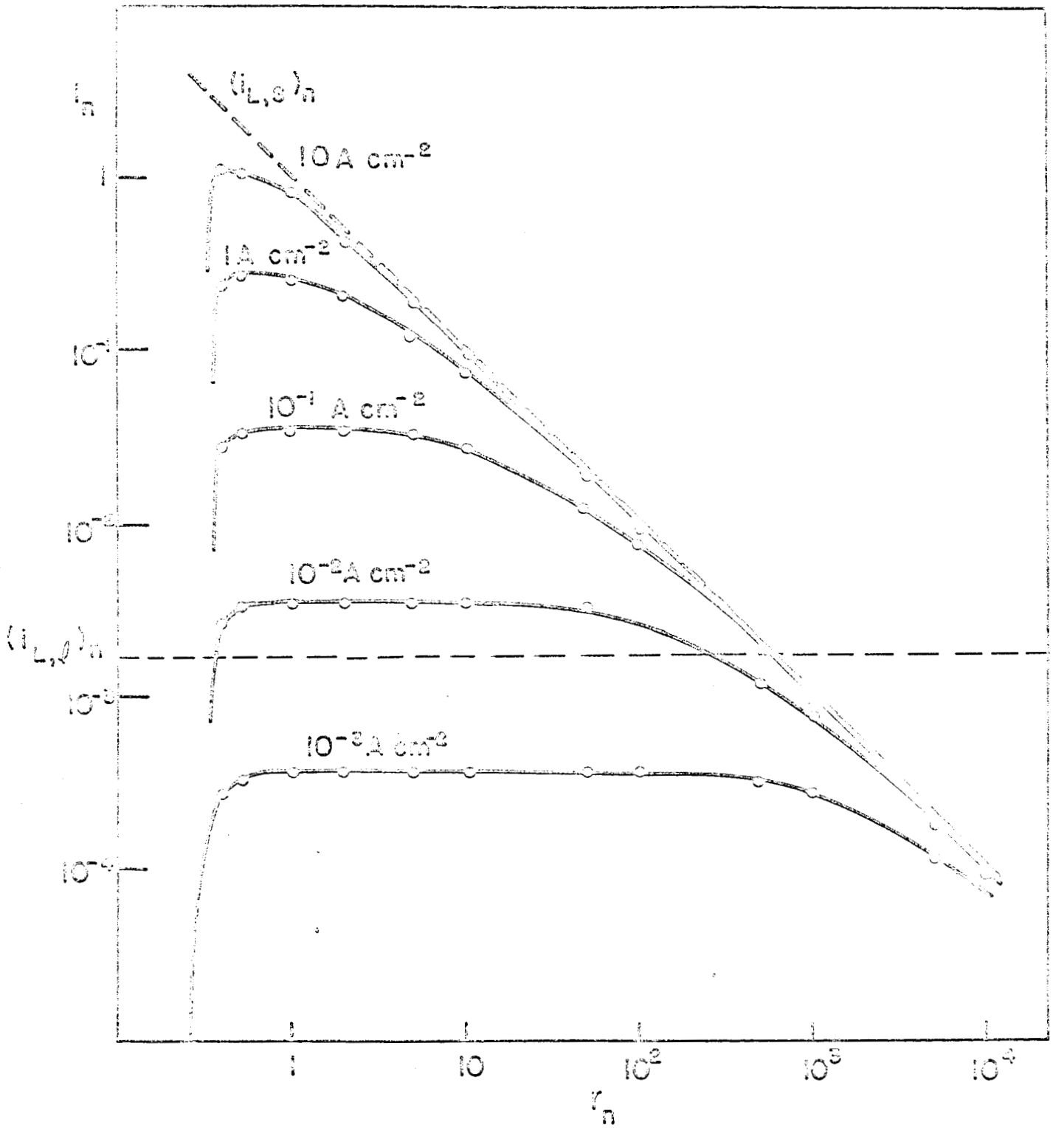
i_n
$(i_{L,s})_n$
10 A cm^{-2}
1
1A cm^{-2}
10^{-1}
10^{-1} A cm^{-2}
10^{-2}
10^{-2}A cm^{-2}
$(i_{L,\ell})_n$
10^{-3}
10^{-3}A cm^{-2}
10^{-4}
1
10
10^2
10^3
10^4
r_n

Fig. 27